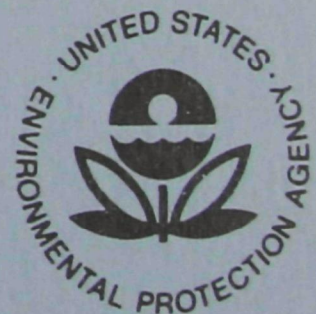


EPA-650/2-74-031-a

April 1974

Environmental Protection Technology Series

**APPLICATION OF HOLOGRAPHIC
METHODS TO THE MEASUREMENT
OF FLAMES AND PARTICULATE,
VOLUME I**



Office of Research and Development
U.S. Environmental Protection Agency
Washington, DC 20460

APPLICATION OF HOLOGRAPHIC METHODS TO THE MEASUREMENT OF FLAMES AND PARTICULATE, VOLUME I

by

A.B. Witte and D.E. Haflinger

TRW Systems Group
One Space Park
Redondo Beach, California 90278

Contract No. 68-02-0603
ROAP No. 21ADG-51
Program Element No. 1AB014

Project Officer: William B. Kuykendal
Control Systems Laboratory
National Environmental Research Center
Research Triangle Park, N. C. 27711

Prepared for

OFFICE OF RESEARCH AND DEVELOPMENT
ENVIRONMENTAL PROTECTION AGENCY
WASHINGTON, D.C. 20460

April 1974

This report has been reviewed by the Environmental Protection Agency and approved for publication. Approval does not signify that the contents necessarily reflect the views and policies of the Agency, nor does mention of trade names or commercial products constitute endorsement or recommendation for use.

TRW REPORT NO. 23523-6001-TU-00

APPLICATION OF HOLOGRAPHIC METHODS
TO THE
MEASUREMENT OF FLAMES AND PARTICULATE

VOLUME I

Prepared for
OFFICE OF RESEARCH AND DEVELOPMENT
ENVIRONMENTAL PROTECTION AGENCY
Washington, D.C. 20460

ABSTRACT

The report gives results of the application of a pulsed ruby laser holographic interferometer to the study of flames, in hopes of extracting temperature profile data. The principle involved is to record holographically the interferogram which presents a three-dimensional record of the interference fringe pattern. The density profile and hence the temperature profile can be calculated from the fringe shift information. The report presents data for a methane-air burner operating both as a diffusion flame and as a premixed flame. The large number of fringe shifts recorded on an interferogram complicated the reduction of the methane-air data, but it was possible to correlate the interferometrically derived temperature data with thermocouple measurements. Application of the technique to a 0.2 gal/hr oil burner was unsuccessful because the highly turbulent flame caused an interference pattern that could not be deciphered. This report was submitted in fulfillment of TRW Project No. 23523 and Contract No. 68-02-0603 by TRW Systems Group under the sponsorship of the Environmental Protection Agency. Work was completed as of November 1973.

CONTENTS

	<u>Page</u>
1. INTRODUCTION.	1
2. EXPERIMENTAL APPARATUS.	3
2.1 Hauck Burner	3
2.2 Methane-Air Burner	4
2.3 Holocamera	5
3. TEST PROCEDURE.	7
4. DATA REDUCTION PROCEDURE.	9
4.1 Introduction	9
4.2 Abel Inversion Technique	9
4.3 Comparison Model to Account for Scene Difference	10
4.4 Premixed Flame Fringe Shift Equation	11
4.5 Diffusion Flame Fringe Shift Equation.	12
4.6 Density Calculation Procedure.	15
4.7 Sample Calculations.	16
4.8 Excess Air Effect.	17
4.9 Velocity Ratio and Reynolds Number	18
5. RESULTS	21
5.1 Sequence of Progress and Problems Solved	21
5.2 Hauck Burner	22
5.3 Flame Interferometry	22
5.4 Premixed Methane-Air Flame	22
5.5 Diffusion Methane-Air Flame.	35
6. CONCLUSIONS AND RECOMMENDATIONS	56
6.1 Conclusions.	56
6.1.1 Interferometric Data Reduction Procedures	56
6.1.2 Diffusion Flame	56
6.1.3 Premixed Flame.	57
6.1.4 Oil Burners	57
6.2 Recommendations.	57
REFERENCES	58

ILLUSTRATIONS

		<u>Page</u>
2-1	Sectional View of Hauck Proportioning Oil Burner and Magnified View of Nozzle Section.	3
2-2	Methane-Air Burner.	4
2-3	Air-Methane Premix Fitting.	5
2-4	Schematic of Holocamera	6
4-1	Diagram of Light Beam	14
4-2	Molecular Weight Versus Excess Air for Methane-Air Combustion.	18
4-3	Gladestone-Dale Constant Versus Excess Air for Methane-Air Combustion.	19
4-4	Methane-Air Burner with Annulus Insert.	20
5-1	Infinite Fringe Interferogram of Methane-Air Burner With Chimney.	23
5-2	Finite Fringe Interferogram of Methane-Air Burner With Chimney.	23
5-3	Infinite Fringe Interferogram of Methane-Air Burner Without Chimney	24
5-4	Finite Fringe Interferogram of Methane-Air Burner Without Chimney	24
5-5	Interferogram of Pre-Mixed Flame With Condition Shown in Table 5-1.	25
5-6	Interferogram of Pre-Mixed Flame With Condition Shown in Table 5-1.	25
5-7	Comparison Between Equations (4-5) and (4-6) for Interferogram Data EPA No. 5-5.	27
5-8	Fringe Shift for Interferogram No. 5-5.	28
5-9	Density Solution for Interferogram EPA No. 5-6.	29
5-10	Fringe Shift for Interferogram EPA No. 5-6.	30
5-11	Effect of Excess Air on Density Profiles for Interferogram No. 5-6	31

ILLUSTRATIONS (Continued)

		<u>Page</u>
5-12	Test Interferogram for Rectangular Box with Pyrex Windows.	32
5-13	Effect of Wall Temperature on Density Profile for Interferogram No. 5-6.	33
5-14	Interferogram with Thermocouples Attached.	34
5-15	Temperature of Methane Air Premixed Flame Versus Percent Excess Air Assumed	36
5-16	Partial Pressures of Combustion Products	37
5-17	Density Profile for Interferogram No. 5-14 With 14 Percent Excess Air.	40
5-18	Schematic of Typical Fringe Pattern Divided Into Its Three Compositional Regions.	42
5-19	Reconstructed Interferogram.	42
5-20	Reconstructed Interferogram.	43
5-21	Reconstructed Interferogram.	43
5-22	Reconstructed Interferogram.	43
5-23	Reconstructed Interferogram.	43
5-24	Reconstructed Interferogram.	43
5-25	Reconstructed Interferogram.	44
5-26	Reconstructed Interferogram.	44
5-27	Reconstructed Interferogram.	44
5-28	Reconstructed Interferogram.	44
5-29	Reconstructed Interferogram.	44
5-30	Reconstructed Interferogram.	46
5-31	Reconstructed Interferogram.	46
5-32	Reconstructed Interferogram.	46
5-33	Reconstructed Interferogram.	46

ILLUSTRATIONS (Continued)

		<u>Page</u>
5-34	Reconstructed Interferogram.	46
5-35	Reconstructed Interferogram.	47
5-36	Reconstructed Interferogram.	47
5-37	Reconstructed Interferogram.	47
5-38	Reconstructed Interferogram.	47
5-39	Reconstructed Interferogram.	47
5-40	Plot of Peak Temperatures of Reduced Interferograms and Thermocouple Data.	49
5-41	Temperatures Profiles With $r = 0.825$ inch, Varying Reynolds Number, Constant UA/UF.	50
5-42	Temperature Profiles with $r = 0.825$ inch, Medium Reynolds Number, Varying UA/UF	51
5-43	Temperature Profiles with $r = 0.825$ inch, High Reynolds Number, Varying UA/UF	52
5-44	Temperature Profiles with $r = 0.4$ inch, Medium Reynolds Number, Varying UA/UF.	53
5-45	Temperature Profiles with $r = 0.4$ inch, High Reynolds Number, Varying UA/UF.	54

TABLES

5-1	Test Condition for Interferograms.	26
5-2	Test Conditions for Diffusion Flame With Radius of Annulus Equal to 0.825 Inch.	39
5-3	Test Conditions for Diffusion Flame With Inner Radius of Annulus Equal to 0.4 Inch	39

ACKNOWLEDGMENTS

Work on this contract was accomplished by personnel of the TRW Fluid Mechanics Laboratory. The Principal Investigator was Dr. Arvel B. Witte; the Project Engineer, Donald E. Haflinger. The TRW Project Manager was Birch J. Matthews. Technical direction and administration of the contract for the Environmental Protection Agency was the responsibility of Mr. William B. Kuykendal.

The authors wish to thank Messrs. Frank Gomes and Robert Briones of the TRW Fluid Mechanics Laboratory for their assistance in conducting the holography experiments. In addition, the assistance and cooperation of Mr. Blair Martin of the Environmental Protection Agency was greatly appreciated.

Metric System Conversion Table

SYMBOL	WHEN YOU KNOW	MULTIPLY BY	TO FIND	SYMBOL
in.	inches	25.4	millimeters	mm
ft	feet	0.3048	meters	m
yd	yards	0.9144	meters	m
lb	pounds	0.453592	kilograms	kg
°F	Fahrenheit temperature	$\frac{5}{9}$ (after subtracting 32)	Celsius temperature	°C
psi	pounds per square inch	51.71	torr	torr
mm	millimeters	0.03937	inches	in.
m	meters	3.28084	feet	ft
m	meters	1.09361	yards	yd
kg	kilograms	2.20462	pounds	lb
°C	Celsius temperature	$\frac{9}{5}$ (then add 32)	Fahrenheit temperature	°F
torr	torr	0.01933	pounds per square inch	psi

x

1. INTRODUCTION

In situ probes may be used to measure the properties of chemically reacting flows encountered in premixed and diffusion flames. Generally they will disturb the flow to produce conditions not normally existent at that point. They also may require extensive calibration of the probe to make accurate measurements possible. In the current study holographic interferometry was used to "remotely sense" the index of refraction, density and temperature fields associated with these flames. No flow field disturbances were caused in this way.

In order to characterize a flow field uniquely, species composition, two state variables, and one dynamic variable must be known. An interferometer measurement yields the index of refraction field, $n(x,y,z)$. n in turn is a function of species mass fraction, C_i , and density. In equilibrium, C_i can be expressed as a function of two state variables, for example, pressure and temperature, when the initial species fractions are known. For the premixed flame in equilibrium, the state variables and composition can be determined uniquely for low speed flames (constant pressure). Data reduction of the diffusion flame is likely to be more complicated because, although local equilibrium may apply, the species may diffuse as well, leaving the initially unreacted composition at a point unknown. In the present study, techniques are developed using holographic interferometry to characterize flame structure and to obtain density and temperature profiles. With the current technique, averaged measurements are made along a line of sight. Data which exhibit axial symmetry can be reduced to localized quantities (radial profiles) by means of inverting the integral equation for fringe shift, a technique established by Abel and described in Reference 1. For the "not so axially symmetric data" either statistical averaging techniques have to be used or the use of wide-angle holographic interferometry and a more sophisticated 3-D data reduction scheme must be employed. Use of a 3-D reduction technique was first applied to holographic interferometry by Witte² and later applied extensively by Matulka³. The extent to which progress toward data reduction of these flames can be made is discussed in some detail in this study.

Two burner flames were investigated. The first, produced by an oil fuel fired burner by Hauck, yielded far too many fringes -- a condition resulting from the fact that the burner could not be operated satisfactorily at the low range of fuel-air rates. The large number of fringes observed was analogous to that measured in burners of somewhat larger size and reported during an earlier EPA program.⁴ This type of burner is described in the next section; however, the flame was not studied interferometrically because of the fringe resolution problem mentioned above.

The second burner operated on methane and air over a wide range of excess air and as a premixed and diffusion flame. Holographic interferometric data reduction techniques are developed for reducing the interferograms recorded of this burner flame.

2. EXPERIMENTAL APPARATUS

2.1 HAUCK BURNER

A schematic of the Hauck Burner* is shown in Figure 2-1. This burner has a maximum air intake rate of 28 cfm with a maximum fuel intake of 1.2 gph and 0.2 gph minimum. To operate the burner, oil must be supplied at approximately 20 psi to the burner pressure regulator. Oil pressure is regulated to the burner from 2 to 10 psi. A separate air blower is required

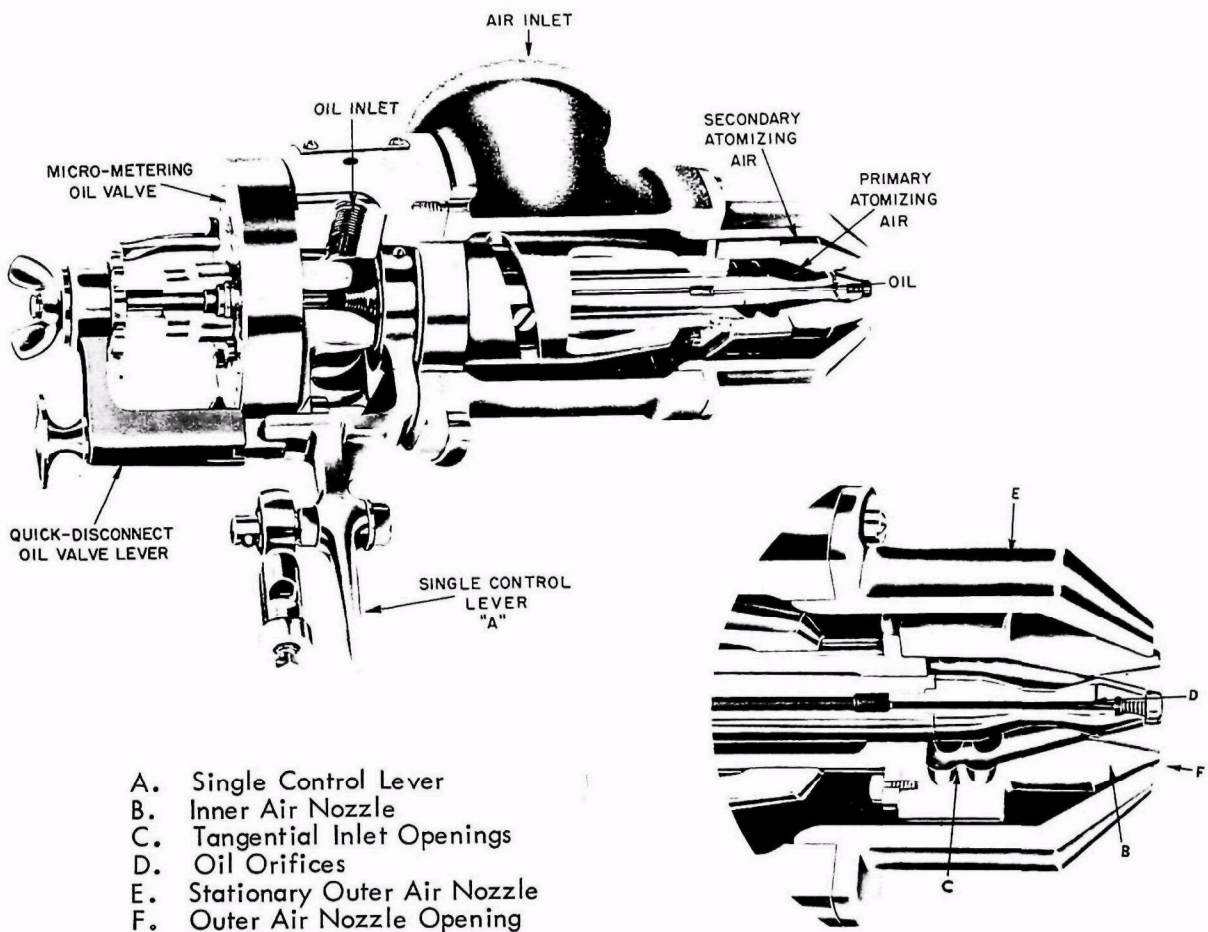


Figure 2-1. Sectional View of Hauck Proportioning Oil Burner and Magnified View of Nozzle Section

*A product of Hauck Manufacturing Co., Lebanon, Pennsylvania.

to supply air at 0.25 psig. The fuel oil was No. 2 distillate obtained from Gulf crude. The oil had an API gravity equal to 36.* The fuel oil was fed to the burner from a small pressurized tank.

2.2 METHANE-AIR BURNER

A schematic of the methane-air burner is shown in Figure 2-2. The design concept for this laboratory methane-air burner was provided by EPA. Additional information was obtained from Prof A.F. Sarofim, Massachusetts Institute of Technology. The burner consists of two concentric cavities into which the air and gaseous fuel are introduced. Both cavities are filled with glass wool to dampen feed system fluctuations and obtain uniform fuel distribution. The air and methane next pass through 12 gauge stainless

steel tube bundle to straighten the flow and break up any large eddies. A screen separates the tube bundle and concentric cavities are housed in a 3.60-inch-diameter tube. Gas and air are injected through a base plate. A retainer ring and four retainer bolts complete the assembly. A glass chimney was initially used to preclude secondary air entrainment into the burner flame. Later the glass chimney was replaced with a thinner quartz chimney for optical reasons. To accomplish a premix flame configuration, methane is introduced into a 1/4-inch-diameter tube which has twenty-five 0.059-inch-diameter holes drilled in it. The tube slips inside a 1/2-inch-diameter bulkhead tee fitting carrying the air. The mixer is shown in Figure 2-3.

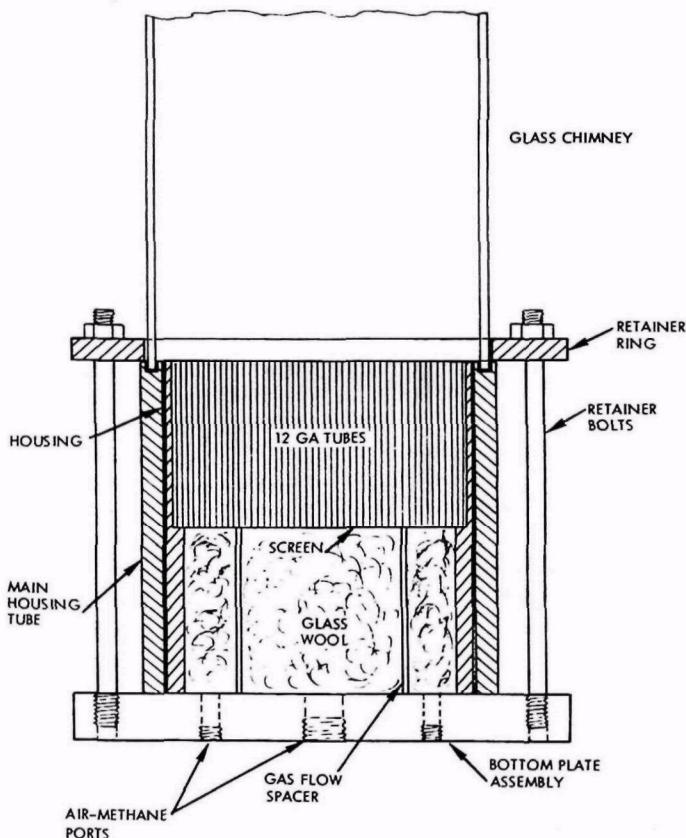


Figure 2-2. Methane-Air Burner

*An API gravity of 36 is equivalent to a specific gravity of 0.845.

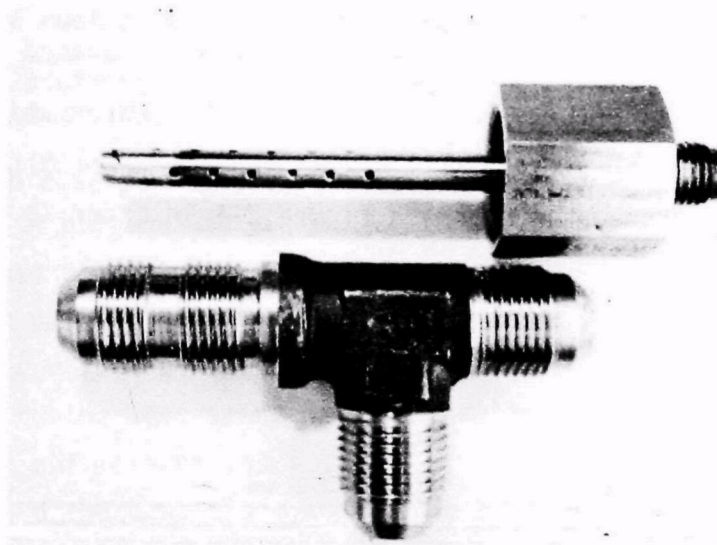


Figure 2-3. Air-Methane Premix Fitting

2.3 HOLOCAMERA

The laser holograph is comprised of a pulsed ruby laser and a holocamera. The pulsed ruby is used in this investigation because sufficient energy can be produced to penetrate the burner flame during a pulse width small enough to stop the action of the combustion phenomena. The pulsed ruby laser has been described in detail in an earlier TRW report to EPA⁴ and will not be discussed further here.

The holocamera design is a modified version of the greater scene depth holocamera used in later series of tests described in Ref. (4). The basic modifications were as follows:

- a) The entire holocamera was rotated 90 degrees to permit insertion of the burner such that burning took place vertically. To have used the previous holocamera configuration would have resulted in contamination of the reference beam by the burner flame and resulting by-products. The flame produced by vertically oriented burner is more nearly symmetric than those at an angle to the gravity field.
- b) A new finite fringe rotator to rotate the hologram vertically, was designed and built to provide horizontal fringes.

- c) The outer pair of lenses from the quadratic lens set, referred to in Ref. (4), was appropriately spaced to produce a focal length of 21 inches, and apertures down to 11 inches in diameter to correct for abbreviations.
- d) Hologram and prism plate were reoriented at 52.5 degrees and 75 degrees as shown on Figure 2-4 in order to reduce reflections.

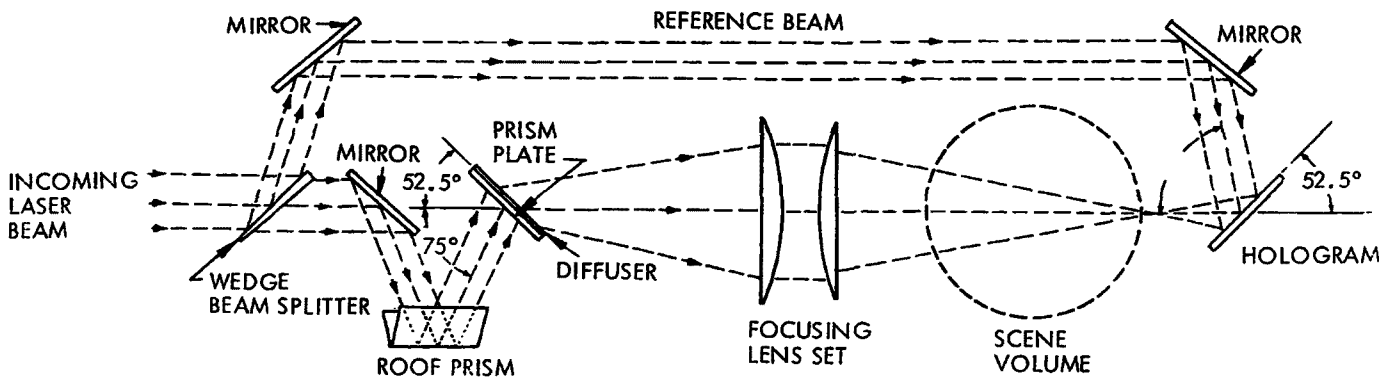


Figure 2-4. Schematic of Holocamera

3. TEST PROCEDURE

A test procedure was established and followed for recording holograms and interferograms of the burner flame. Starting with the burner in place, the following steps were taken to make the recordings:

- 1) Ignite burner
- 2) Adjust regulator pressures and flow rate
- 3) Turn off lights
- 4) Uncover film plate
- 5) Record the test scene holographically
- 6) Shut off methane input
- 7) Record the comparison scene holographically
- 8) Cover film plate
- 9) Lights on
- 10) Develop plate.

Ideally, the comparison scene should be recorded before the test scene; however, with this burner, it was necessary to reverse the order because the quartz chimney had to be removed in order to ignite the burner. Removing the chimney could leave movement fringes in the resulting interferogram.

In the premixed flame configuration, thermocouple readings were recorded during the time the test scene was holographically recorded. Some thermocouple readings were also taken at a later time period. Comparison of thermocouple readings showed that good test-to-test repeatability could be achieved without any loss in accuracy.

In order to save time and also to avoid any obscuration, wall thermocouple readings for the diffusion flame configuration were also recorded at a different time period than the interferogram recordings. The annulus (see Section 2.3) was changed to vary the mixing region thickness as well as overall stoichiometry. This modification simply requires lifting out the center core of the burner.

All of the interferograms and holograms were recorded on Agfa 8E75 anti-halation backed 4' x 5-inch glass plates*. Development time in Eastman Kodak

*Product of Agfa-Gevaert, Antwerp, Belgium.

HRP developer was typically 4 minutes for an interferogram. The acid fixer used was Nacco fix.

Interferograms were reconstructed with a Model 124A Spectra Physics helium neon gas laser ($\lambda = 0.6943\mu$) illuminator. The recordings were photographed using Polaroid Type 52 film, having an ASA rating of 400. When desired, negatives of the reconstructed scene were made using Polaroid Type 55 P/N film.

4. DATA REDUCTION PROCEDURE

4.1 INTRODUCTION

Data reduction is comprised of three parts: photographing the desired view of the holographic interferogram and recording the fringe pattern using a microdensitometer*; interpreting fringe number from the microdensitometer trace; and computing density by means of the standard equation for fringe shift,

$$S(x,y) = \frac{K}{\lambda} \int_0^z \left[\rho(x, y, z) - \rho_{\infty} \right] dz \quad (4-1)$$

The holographic interferogram is mounted in a reconstruction jig whose orientation is the same with respect to the reference beam as it was during the original recording of the holographic interferogram. During reconstruction, a 15 mw continuous wave He-Ne laser ($\lambda = 0.6943$ micron) was used to illuminate the holographic interferogram. A copy camera was positioned behind the holographic interferogram. The camera could be focused on the event which was a known distance behind the holographic interferogram and bounded by the viewing cone of the hologram.

The interferograms were photographed with either Polaroid Type 55 PN film which provides a positive and negative copy of the event using a nominal 1- to 10-second exposure at f/5.6 or Polaroid Type 52 which is about 8 times faster. The photographic density of the fringe pattern on these negatives was then recorded on a Joyce precision microdensitometer having a slit size of about 0.010 inch by 0.010 inch.

4.2 ABEL INVERSION TECHNIQUE

Fringe number S was measured relative to the undisturbed (light fringe) background gas, i.e., relative to $S_{\infty} = 0$. The first dark fringe occurs where the change in optical path is $\lambda/2$. Interpretation of the change in optical path in wavelengths, of light, i.e., fringe number S , is aided by keeping in mind the standard equation for fringe shift. Starting at the

*When many fringes are available, use of the microdensitometer may be unnecessary.

edge of the flame the fringe number begins to decrease, the first dark fringe yielding a value of $S = -1/2$ fringe.

The mean density profile calculations carried out here were made under the assumption that the flow field was axisymmetric. With the assumption of axisymmetric flow, the equation can be inverted as the Abel integral to obtain

$$\rho(y) - \rho_{\infty} = -\frac{\lambda}{\pi K} \int_{y^2}^{r^2} \frac{\frac{ds}{dr^2} dr^2}{(r^2 - y^2)^{1/2}} \quad (4-2)$$

When this equation is rewritten as

$$\rho(y) - \rho_{\infty} = -\frac{\lambda}{\pi K} 2 \int_{y^2}^{r^2} \frac{ds}{dr^2} d(r^2 - y^2)^{1/2} \quad (4-3)$$

it may be cast into the following finite difference form (the Schardin van Voorhis approximation) for which the density is assumed constant in each of N thin angular rings of thickness Δ :

$$\rho(y) - \rho_{\infty} = \frac{2\lambda}{\pi\Delta K} \sum_{k=i}^{N-1} (S_k - S_{k+1}) \frac{\sqrt{(k+1)^2 - i^2} - \sqrt{k^2 - i^2}}{2k+1} \quad (4-4)$$

where $r_k = \Delta k$, $y = \Delta i$ and $r_N = \Delta N$ has been used and the indice i takes on the following values: $i = 0, 1, 2, \dots, N-1$. K is the Gladstone-Dale constant, e.g., for $\rho_{\infty} K = 2.926 \times 10^{-4}$ for air when $\rho_{\infty} = 1$ atm.

4.3 COMPARISON MODEL TO ACCOUNT FOR SCENE DIFFERENCE

Accounts must be made for different chemical species between the double exposures creating the interferograms because the comparison scene is recorded with air and the test scene recorded with combustion products.

Therefore, the Abel Inversion technique was modified to accept β_T and β_∞ by using the Gladstone-Dale equation for a dilute gas. The original program was used to solve the fringe shift equation

$$S = \frac{P_\infty^k}{\lambda} \int \left(\frac{\rho}{\rho_\infty} - 1 \right) dx \quad (4-5)$$

which does not account for the difference in gas composition between the test and comparison beam recordings. By using the Gladstone-Dale relationship, $n - 1 = \beta P/\rho_s$, and the basic fringe shift equation, $S = \frac{1}{\lambda} \int (n - n_\infty) dz$, one gets

$$S = \frac{\beta_\infty}{\lambda} \frac{P_\infty}{\rho_\infty} \int \left(\frac{\beta_T}{\beta_\infty} \frac{P_\infty}{P_{T0}} \frac{\rho}{\rho_\infty} - 1 \right) dx \quad (4-6)$$

which accounts for the difference in composition. The Gladstone-Dale constant for the reaction products of methane-air combustion, β_T , is shown to be 3.208×10^{-4} for stoichiometric conditions.

4.4 PREMIXED FLAME FRINGE SHIFT EQUATION

For the premixed flame configuration, further modification of the fringe shift equation had to be carried out due to the occluded region which appears on the edges of the quartz chimney, an observation which will be discussed later.

This occluded portion of the interferogram at the wall of the quartz chimney had caused concern because initial calculation had indicated a centerline temperature $T/T_\infty \leq 2$ for the premixed configuration, which appeared to be far too low. It was concluded that the fringe shift readings within the occluded region could not accurately be determined. One possible method of alleviating this source of error is to measure the wall temperature of the quartz chimney and to include this additional information in the fringe shift equation. By rearranging the fringe equation,

$$S = \frac{1}{\lambda} \int (n - n_\infty) dz \quad (4-7)$$

into two separate integrals and considering the wall temperature, then

$$S = \frac{1}{\lambda} \int (n - n_w) dz + \frac{1}{\lambda} \int (n_w - n_\infty) dz \quad (4-8)$$

Now, again, using the Gladstone-Dale relationship, it can be shown that the fringe shift equation is:

$$S = \frac{\beta_T}{\lambda} \frac{\rho_\infty}{\rho_{T_0}} \int \left(\frac{\rho_\infty}{\rho_{T_0}} \frac{\rho}{\rho_\infty} - 1 \right) dz - 2 \frac{\beta_\infty}{\lambda} \frac{\rho_\infty}{\rho_{\infty 0}} \left(\frac{\beta_T}{\beta_\infty} \frac{\rho_{\infty 0}}{\rho_\infty} \frac{\rho_w}{\rho_{T_0}} - 1 \right) \left[r_0 - (r_0^2 - r^2)^{1/2} \right] \quad (4-9)$$

4.5 DIFFUSION FLAME FRINGE SHIFT EQUATION

In the diffusion flame configuration, the same occluded region appears on the recorded interferograms and, therefore, the fringe shift equation has to be modified in a similar manner as presented above. However, there is an additional consideration that must be taken into account. In the case of the diffusion flame, the Gladstone-Dale constant is no longer uniform across the chimney region and, therefore, must be varied in the evaluation of the fringe shift equation. In the outer portion of the chimney, there is air with no unburned fuel nor combustion products. Moving towards the center of the chimney region, combustion products are encountered, and, finally, at the center of the quartz chimney, the gases are probably a mixture of unburned fuel with some combustion products. To evaluate the fringe shift equation, the following modification (which is shown in greater detail than previously) must be made for the different species configuration. The general fringe number equation is

$$S = \frac{1}{\lambda} \int (n - n_\infty)$$

Now, separating this equation into two separate integrals as before we get

$$S = \frac{1}{\lambda} \left[\int (n - n_w) dz + \int (n_w - n_\infty) dz \right] \quad (4-10)$$

Using the Gladstone-Dale relationship, $n = 1 + \beta \rho/\rho_s$, such that

$$n = \beta_T \frac{\rho}{\rho_{0T}} + 1 \quad (\text{species condition})$$

$$n_w = \beta_\infty \frac{\rho_w}{\rho_{\infty 0}} + 1 \quad (\text{wall condition})$$

and

$$n_\infty = \beta_\infty \frac{\rho}{\rho_{\infty 0}} \quad (\text{reference condition})$$

and substituting these relationships into the fringe number equation, one gets

$$\begin{aligned} \frac{1}{\lambda} \int (n - n_\infty) dz &= \frac{1}{\lambda} \int \left[\left(\beta_T \frac{\rho}{\rho_{0T}} + 1 \right) - \left(\beta_\infty \frac{\rho_w}{\rho_{\infty 0}} + 1 \right) \right] dz \\ &+ \frac{1}{\lambda} \int \left[\left(\beta_\infty \frac{\rho_w}{\rho_{\infty 0}} + 1 \right) - \left(\beta_\infty \frac{\rho}{\rho_{\infty 0}} + 1 \right) \right] dz \\ &= \frac{\beta_\infty}{\lambda} \int \left(\frac{\beta_T}{\beta_\infty} \frac{\rho}{\rho_{0T}} - \frac{\rho_w}{\rho_{\infty 0}} \right) dz + \frac{\beta_\infty}{\lambda} \left(\frac{\rho_w}{\rho_{\infty 0}} - \frac{\rho}{\rho_{\infty 0}} \right) \int dz \end{aligned} \quad (4-11)$$

After some algebra

$$S = \frac{\beta_\infty}{\lambda} \frac{\rho_{\infty 0}}{\rho_{\infty 0}} \frac{\rho_w}{\rho_{\infty 0}} \int \left(\frac{\beta_T}{\beta_\infty} \frac{\rho_{\infty 0}}{\rho_{0T}} \frac{\rho_{\infty 0}}{\rho_w} \frac{\rho}{\rho_{\infty 0}} - 1 \right) dz + \frac{\beta_\infty}{\lambda} \frac{\rho_{\infty 0}}{\rho_{\infty 0}} \left(\frac{\rho_w}{\rho_{\infty 0}} - 1 \right) \int dz \quad (4-12)$$

The integral $\int dz$ can be transformed into terms of r/r_0 as can be seen by referring to Figure 4-1.

$$\int dz = -2 \int \left[r_0^2 - (r_0^2 - r^2)^{1/2} \right] dr \quad (4-13)$$

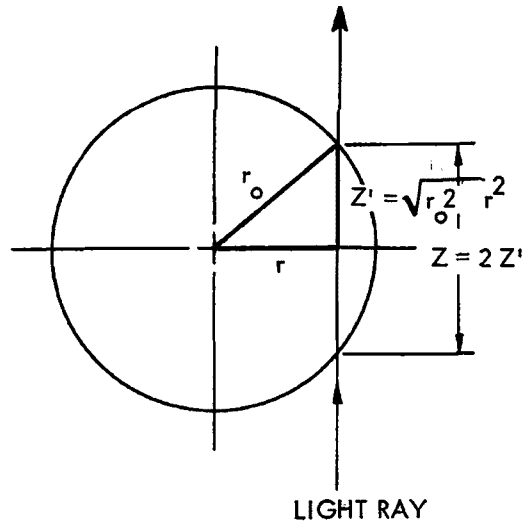


Figure 4-1. Diagram of Light Beam

and therefore

$$S = \frac{\beta_{\infty}}{\lambda} \frac{\rho_{\infty}}{\rho_0} \frac{\rho_w}{\rho_{\infty}} \int \left(\frac{\rho_{\tau}}{\beta_{\infty}} \frac{\rho_{\infty 0}}{\rho_{0\tau}} \frac{\rho_{\infty}}{\rho_w} \frac{\rho}{\rho_{\infty}} - 1 \right) dz = 2 \frac{\beta_{\infty}}{\lambda} \frac{\rho_{\infty}}{\rho_0} \left(\frac{\rho_w}{\rho_{\infty}} - 1 \right) \left[r_0 - (r_0^2 - r^2)^{1/2} \right] \quad (4-14)$$

where

S = fringe shift

λ = irradiation wavelength

β = Gladstone-Date constant

ρ = density

z = distance along light ray

subscripts: ∞ = comparison scene condition of air burner is turned off

τ = local test scene condition (which varies for diffusion flame configuration and is constant having combustion product species for premixed flame configuration)

o = standard conditions at which β 's are evaluated

w = wall conditions

4.6 DENSITY CALCULATION PROCEDURE

The procedure for both the premixed flame configuration and the diffusion flame is about the same. First, correct the fringe numbers by adding the function $\chi \cdot \left[r_o - (r_o^2 - r^2)^{1/2} \right]$ where,

$$\chi_p = 2 \frac{\beta_\infty}{\lambda} \frac{\rho_\infty}{\rho_{\infty 0}} \left(\frac{\beta_T}{\beta_\infty} \frac{\rho_{\infty 0}}{\rho_\infty} \frac{\rho_w}{\rho_{T 0}} - 1 \right) \quad (4-15-1) \quad (\text{premixed})$$

$$\chi_d = 2 \frac{\beta_\infty}{\lambda} \frac{\rho_\infty}{\rho_{\infty 0}} \left(\frac{\rho_w}{\rho_\infty} - 1 \right) \quad (4-15-2) \quad (\text{diffusion})$$

Now, calculate the quantity

$$Y_p = \frac{\rho_{\infty 0}}{\rho_{T 0}} \quad (4-16-1) \quad (\text{premixed})$$

$$Y_d = \frac{\beta_T}{\beta_\infty} \frac{\rho_{\infty 0}}{\rho_{T 0}} \frac{\rho_\infty}{\rho_w} \quad (4-16-2) \quad (\text{diffusion})$$

Then dividing by the appropriate Y quantity one gets the density ratio, ρ/ρ_∞ , which is the flame density normalized by the density at the conditions of the comparison scene recording (room temperature and pressure).

The value of β is calculated as follows from the Gladstone-Dale equation for species $i = 1, 2 \dots N$. For any dilute gas,

$$n - 1 = \sum \beta_i \frac{\rho_i}{\rho_{oi}} \quad (4-17)$$

$$= \rho \sum \frac{\beta_i}{\rho_{oi}} C_i \quad (4-18)$$

where β_i is evaluated for species i and C_i is the mass fraction. However, by definition

$$n - 1 = \beta_T \frac{\rho}{\rho_{OT}} \quad (4-19)$$

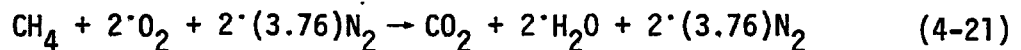
Therefore, combining these two equations yields

$$\beta_T = \rho_{OT} \sum \frac{C_i \beta_i}{\rho_{oi}} \quad (4-20)$$

ρ_{oi} can be shown to be $0.00279 m_i \text{ lb}_m/\text{ft}^3$ at atmospheric pressure and 0°C where m_i is the molecular weight of species i .

4.7 SAMPLE CALCULATIONS

As an example, consider the chemical reaction of premixed methane-air combustion at stoichiometric conditions



From this reaction, the following is calculated:

Reactions Products	Number of Moles (N)	Molecular Weight (m)	N x m	Mass fraction (c_i)
CO ₂	1	44	44	0.1541
H ₂ O	2	18	36	0.1261
N ₂	7.34	28	<u>205.52</u>	<u>0.7198</u>
			285.52	1.0000

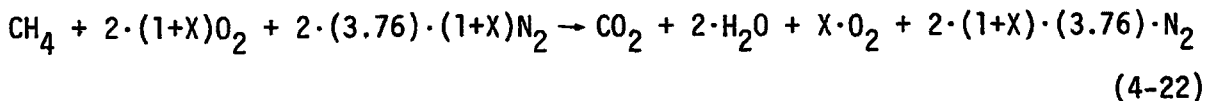
Reactions Products	c_i	β_i	ρ_{oi}	β_i/ρ_{oi}	$c_i \rho_{oi}$	$c_i \beta_i/\rho_{oi}$
CO ₂	0.1541	4.51×10^{-4}	0.12276	3.674×10^{-3}	.0189	5.662×10^{-4}
H ₂ O	0.1261	2.54×10^{-4}	0.05022	5.058×10^{-3}	.00633	6.378×10^{-4}
N ₂	0.7198	2.97×10^{-4}	0.07812	3.802×10^{-3}	.05623	2.737×10^{-3}

The following useful parameters can also be calculated:

Parameter	Equation	Value
ρ_o	$= \sum C_i \rho_{o_i}$	$0.0814 \text{ lb}_m/\text{ft}^3$
	$\sum C_i (\beta_i/\rho_{o_i})$	$= 3.941 \times 10^{-3}$
β_T	$= (0.814) (3.941 \times 10^{-3})$	$= 3.208 \times 10^{-4}$
β_∞	(for air)	$= 2.926 \times 10^{-4}$
$1/\bar{m}$	$\sum C_i/m_i$	0.03621
\bar{m}		$= 27.6$
\bar{m}_a	(for air)	$= 28.83$
$\rho_{\infty o}/\rho_{T o}$	$= \bar{m}/\bar{m}_a$	$= 1.0446$
$\rho_\infty/\rho_{\infty o}$	$= T_{\infty o}/T_\infty$	$= 0.9286$
$\frac{\beta_T}{\beta_\infty} \frac{\rho_{\infty o}}{\rho_{T o}}$		$= 1.14$

4.8 EXCESS AIR EFFECT

The conditions calculated previously were for stoichiometric combustion. It is assumed that combustion is complete. However, since complete combustion is not probable, excess air is added to insure complete combustion of methane (CH_4) to form the reaction products of carbon dioxide (CO_2) and water vapor (H_2O). This addition of "excess air" affects the molecular weight of the reaction products as shown in Figure 4-2. The reaction equation which includes excess air reads as follows:



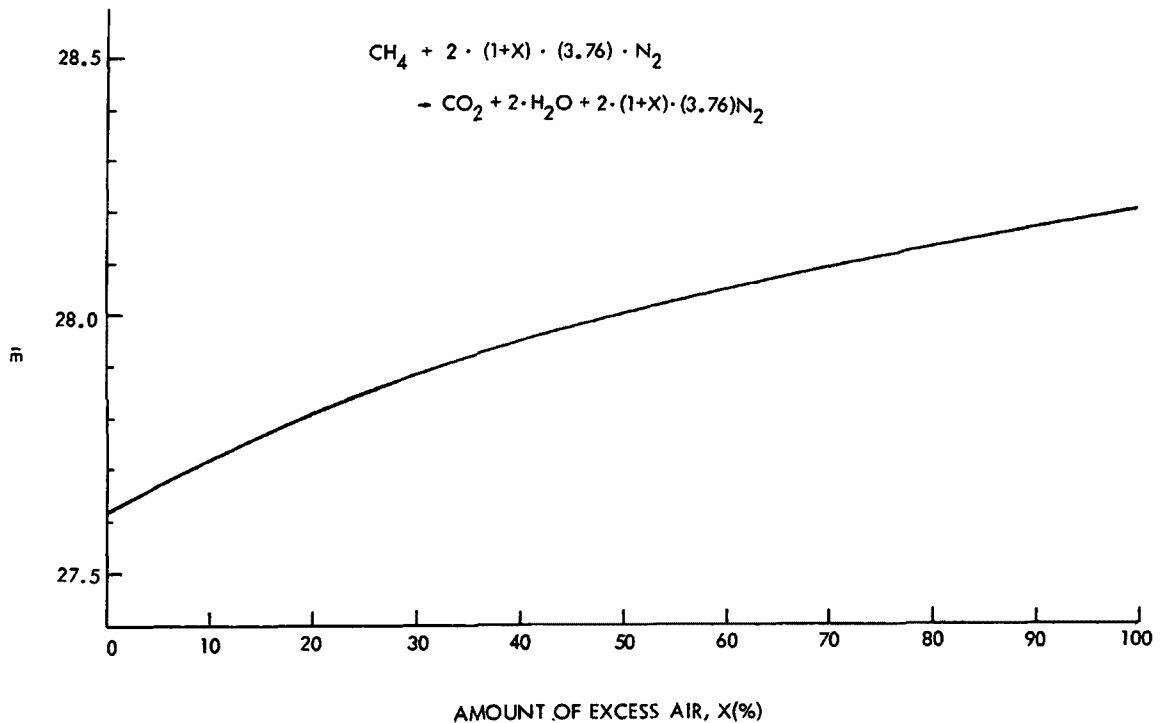


Figure 4-2. Molecular Weight Versus Excess Air for Methane-Air Combustion

where X is the amount of excess air. Excess air is usually defined in terms of percent of theoretical air, such that:

$$X = \frac{\text{AIR}_{\text{actual}} - \text{AIR}_{\text{theoretical}}}{\text{AIR}_{\text{theoretical}}} \times 100\% \quad (4-23)$$

The amount of excess air also affects the Gladstone-Dale constant, β_T , for the resultant reaction product which is shown in Figure 4-3.

4.9 VELOCITY RATIO AND REYNOLDS NUMBER

For diffusion flames, two parameters should be defined: (1) the velocity ratio, and (2) Reynolds number.

The velocity ratio is defined as

$$\frac{U_a}{U_f} = \frac{Q_a A_f}{Q_f A_a} = \frac{Q_a \pi r^2}{Q_f \pi (R^2 - r^2)} \quad (4-24)$$

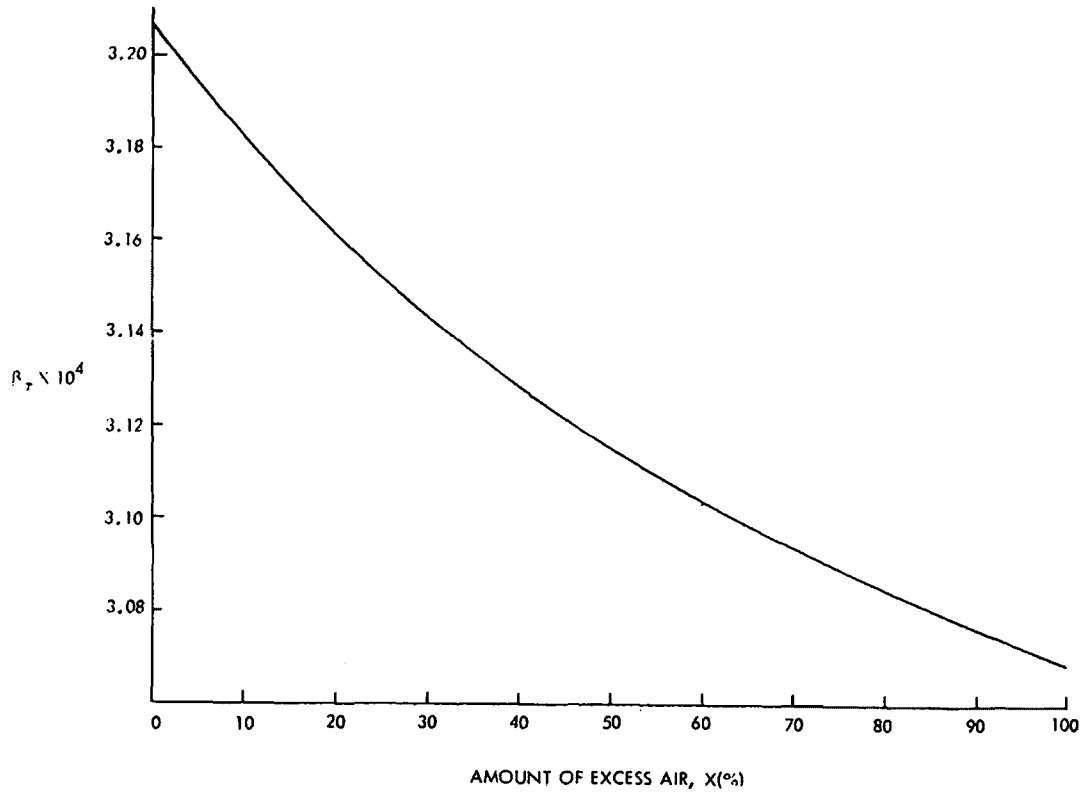


Figure 4-3. Gladstone-Dale Constant Versus Excess Air for Methane-Air Combustion

where r is the annulus radius, R is the burner radius (see Figure 4-4). Q_a is the air flow rate and Q_f is the methane flow rate.

The Reynolds number is defined as

$$R_e = \frac{\rho_\infty \bar{u} L}{\mu_\infty} \quad (4-25)$$

where the density and viscosity are defined at room temperature and pressure, \bar{u} , is the average velocity of air and methane ($u = [u_a + u_f]/2$), and L is the distance above the burner surface at which the data are being reduced.

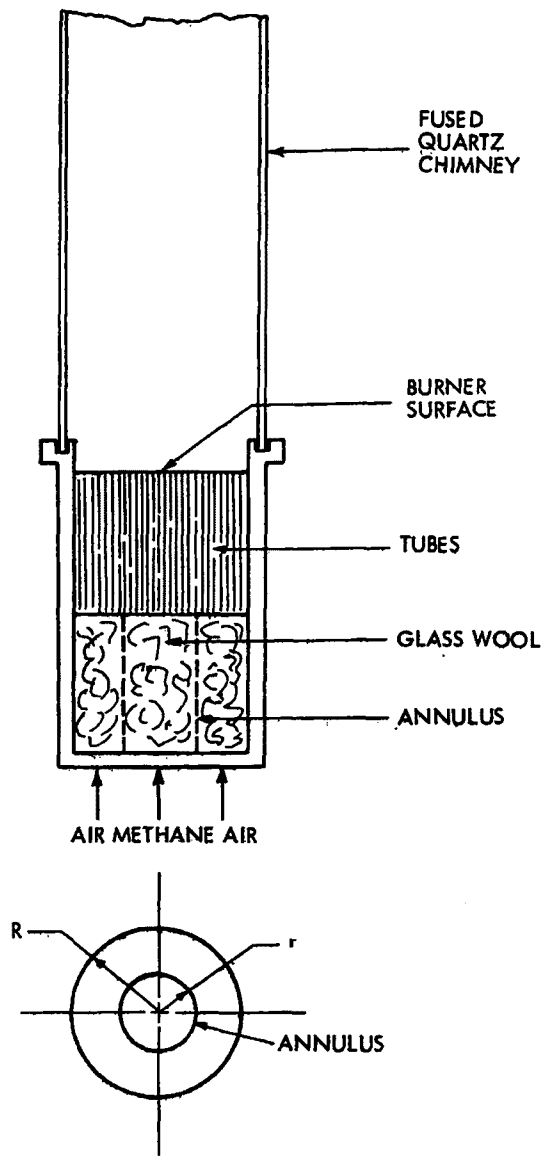


Figure 4-4. Methane-Air Burner With Annulus Insert

5. RESULTS

5.1 SEQUENCE OF PROGRESS AND PROBLEMS SOLVED

Before proceeding with a discussion of the results, a chronological perspective of the progress and problems leading to those results will be given. The following areas were investigated and progress made as indicated:

- Methane burner was fabricated for use in creating both premixed and diffusion flames.
- Finite fringe and infinite fringe interferograms were recorded in diffusion flame configuration.
- Occluded region was greatly reduced.
- Laminar premixed flame was easy to produce.
- Finite fringe interferograms were recorded of premixed flame.
- Modification of data reduction procedure to eliminate occluded region problem was accomplished.
- Centerline and wall thermocouple temperature measurements were made of the premixed flame.
- Data reduction of the interferograms for the premixed flame was accomplished.
- Finite fringe interferograms were recorded of diffusion flame.
- Film fogging problem (during high flow rates in diffusion flame tests) solved with filters.
- Wall thermocouple temperature measurements were made of the diffusion flame.
- Data reduction of the interferogram for diffusion flame was accomplished.
- Both laminar and turbulent flames were observed in the diffusion flame configuration.

5.2 HAUCK BURNER

A small size (as low as 0.2 gph) fuel oil-fired burner was selected for study because it represents a compromise between the large (1 gph) burners tested during a previous EPA study and the methane-air burner which is an approximation to the oil-fired burner for the purpose of instrumentation development. During testing of this burner, it was found that the flow rate, turbulence, and illumination were much larger than expected. It was then decided that the concentration of efforts should be placed on the methane-air burner, because no new information could be obtained with this Hauck burner.

5.3 FLAME INTERFEROMETRY

Holographic interferograms of methane-air combustion were recorded to ascertain what problems might be encountered in obtaining good quality reconstruction. Infinite and finite fringe recordings were made both with and without the glass (Pyrex) chimney. Figures 5-1 through 5-4 show the results of these initial interferograms of a diffusion flame. These figures indicate that finite fringe interferograms would be best suited for this study. Also, the requirement to control the ratio of fuel to oxidizer dictated the need to use the chimney even though the occluded region caused additional problems in reducing the fringe pattern. Note condensation in Figure 5-1.

5.4 PREMIXED METHANE-AIR FLAME

In the premixed configuration, initial tests were conducted under stable flame conditions. A stable flame is defined as a steady blue-violet flame which is attached at the burner surface. It was found that when the fuel mixture was too rich^{*}, the flame would rise up the chimney and go out. In the opposite condition, when the fuel mixture was too lean, the flame had the tendency to be "blown" out. Over the range of allowed operating conditions a laminar-like flame was observed.

Initial holographic interferograms recorded are shown in Figures 5-5 and 5-6, with test conditions shown in Table 5-1. These interferograms are used to show the effects of the various modifications of the data reduction procedure results.

*"Rich" in this case may be a misleading term since all flames were operated with some excess air. This burner would not operate under true rich fuel conditions.

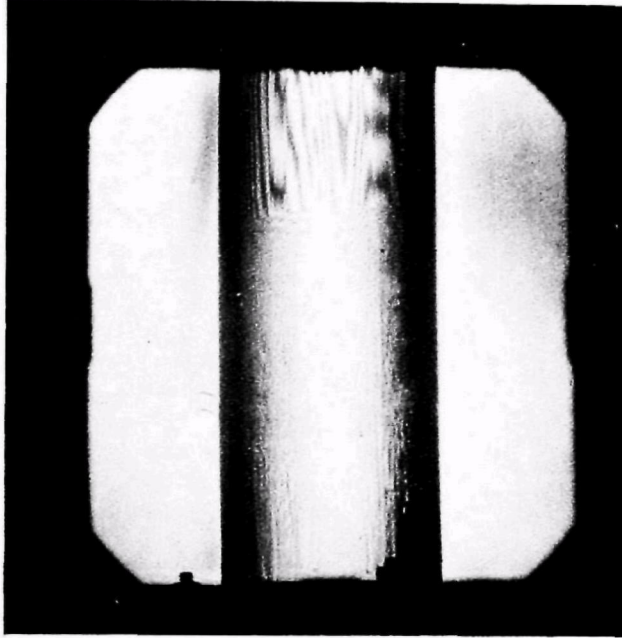


Figure 5-1. Infinite Fringe Interferogram of Methane-Air Burner With Chimney

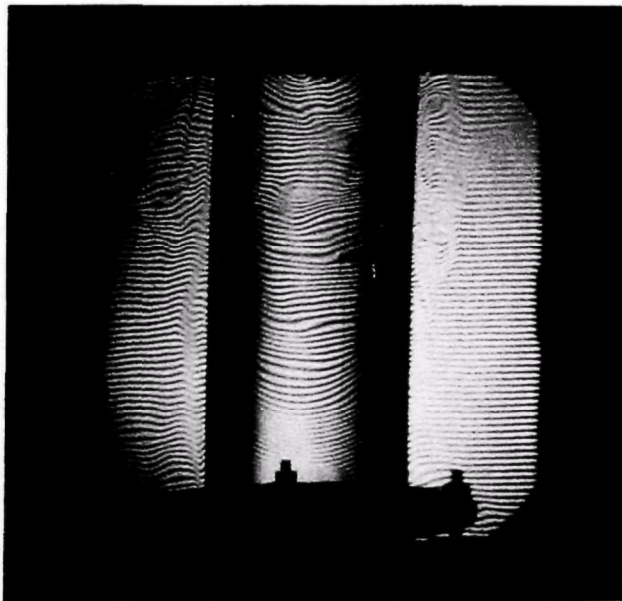


Figure 5-2. Finite Fringe Interferogram of Methane-Air Burner With Chimney

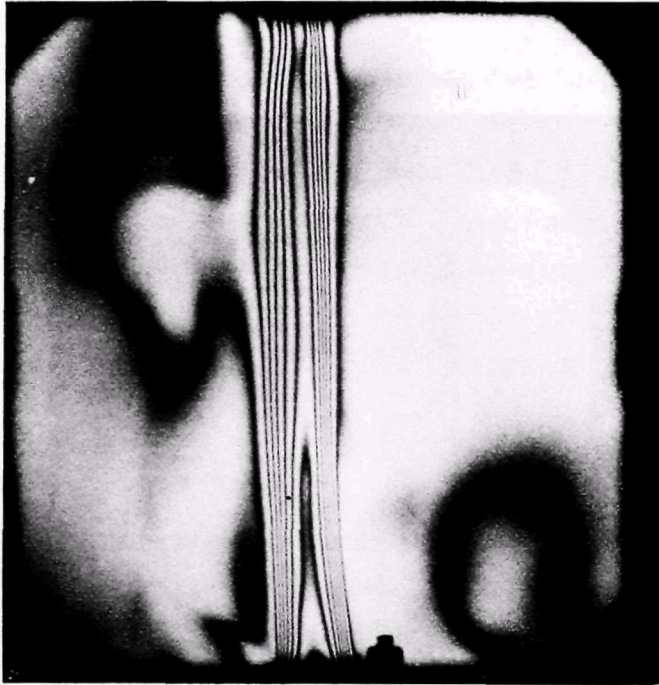


Figure 5-3. Infinite Fringe Interferogram of Methane-Air Burner Without Chimney

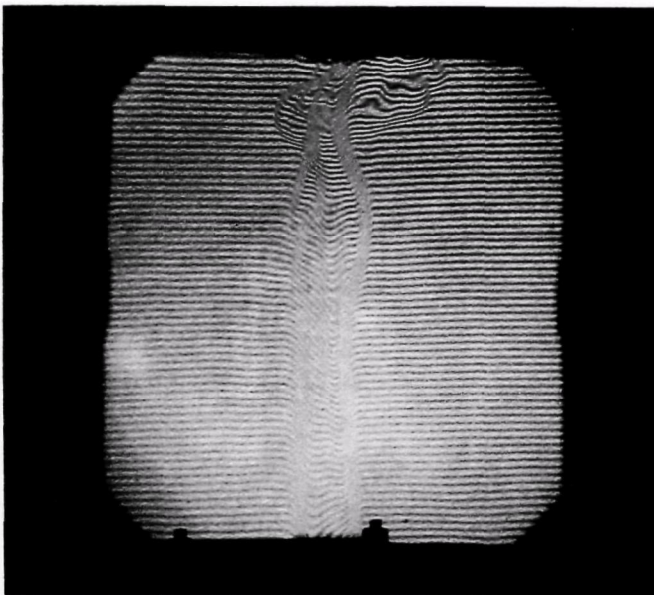


Figure 5-4. Finite Fringe Interferogram of Methane-Air Burner Without Chimney

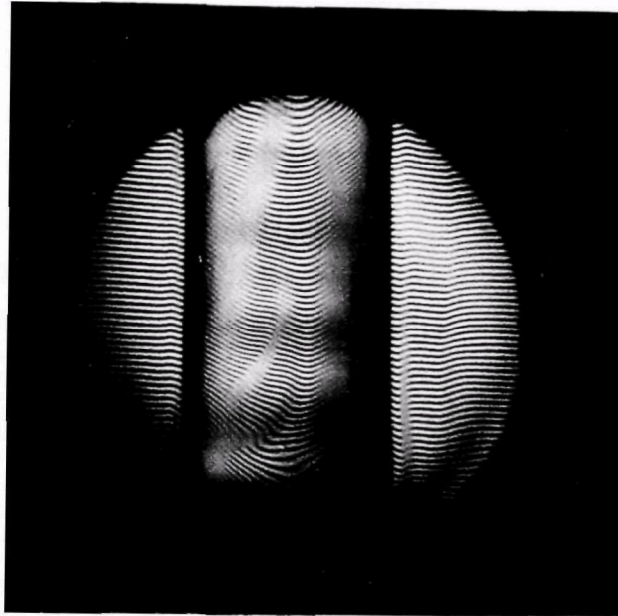


Figure 5-5. Interferogram of Pre-mixed Flame With Condition Shown in Table 5-1

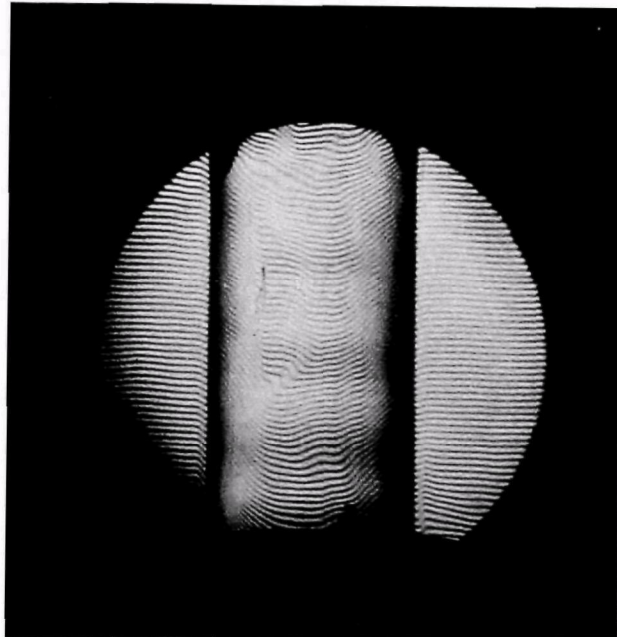


Figure 5-6. Interferogram of Pre-mixed Flame With Condition Shown in Table 5-1

Table 5-1. Test Condition for Interferograms

Hologram Number	Air		Methane		Conditions	Remarks
	Regulator Pressure	Flow Meter	Regulator Pressure	Flow Meter		
5-5	30 psig	16800 cc/min	30 psig	1200 + cc/min	S.S. screen quartz stack	Air flowing for no fire condition
5-6	30 psig	16800 cc/min	30 psig	930 cc/min	No screen stack on	Low flame no popping

A comparison between Equations (4-5) and (4-6), as shown in Section 4, is made in Figure 5-7. The solid curve is the density profile for interferogram 5-5* using Equation (4-5) for which hot and cold combustion gases occur in the test and comparison scenes, respectively. The dashed curve represents Equation (4-6) in which account is made of the change in index between scene recordings. The fringe shift profile used for this comparison is shown in Figure 5-8. As can be seen in Figure 5-7, this first modification tends to slightly lower the resulting density profile as compared with the original fringe shift equation.

Note the discontinuity of the density profile at the centerline. This discontinuity ($r/r_0 = 0$ of Figure 5-7) can be explained by examining the S-curve of Figure 5-8. The maximum in the S-curve is to the left of center, such that $ds/dr_{r/r_0 = 0} \neq 0$. The inverted fringe shift equation for density

$$\frac{\rho(y)}{\rho_\infty} = 1 - \frac{\lambda}{\pi \kappa \rho_\infty} \int_y^{r_s} \frac{\frac{ds}{dr} dr^2}{(r^2 - y^2)^{1/2}}$$

shows that with a negative $ds/dr|_{r/r_0 = 0}$ the density will be initially larger than if the $ds/dr_{r/r_0 = 0}$ is positive. Thus, the density is discontinuous as r approaches $r = 0$, a condition which is physically impossible

* Interferograms will be identified by their figure number.

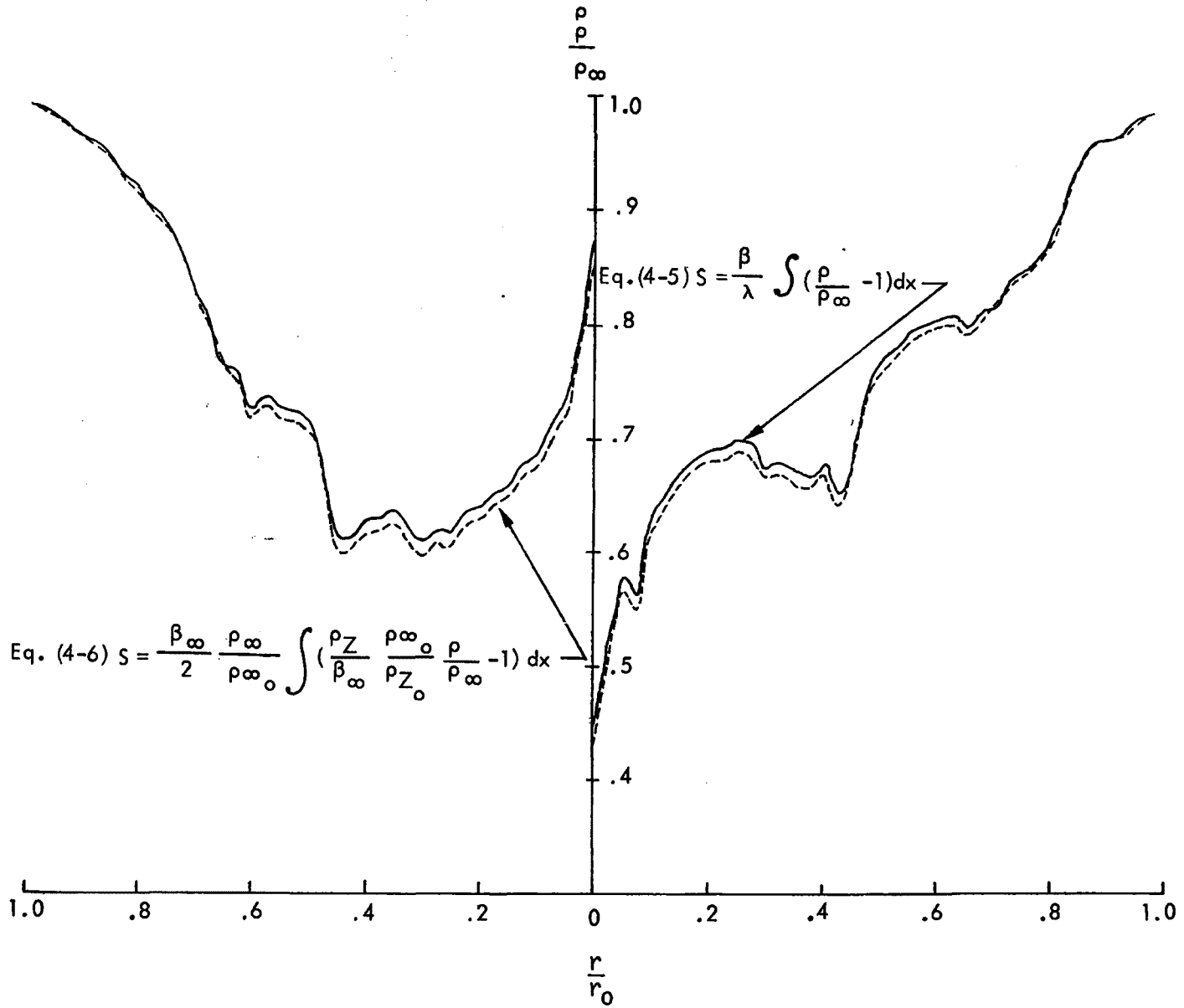


Figure 5-7. Comparison Between Equations (4-5) and (4-6) for Interferogram Data EPA No. 5-5

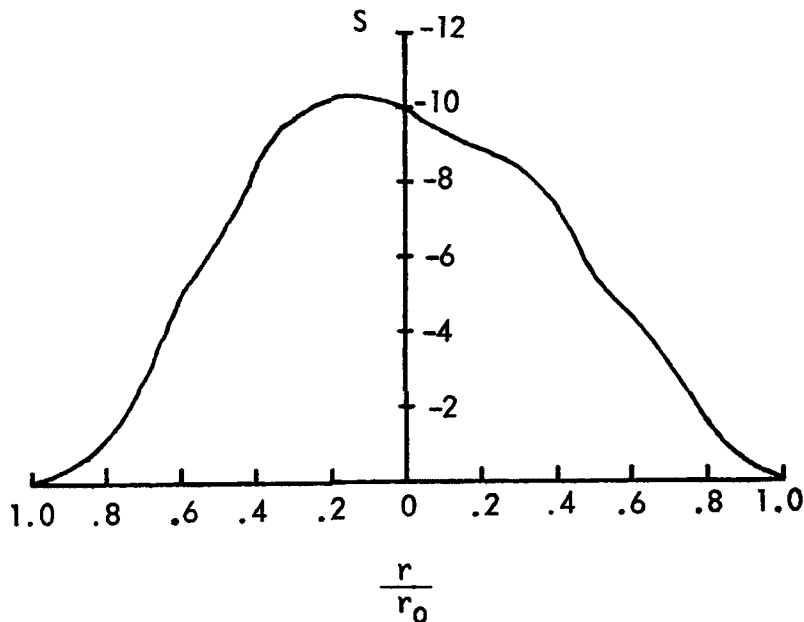


Figure 5-8. Fringe Shift for Interferogram No. 5-5

for this flow problem. Figure 5-9 shows a similar phenomenon for interferogram 5-6. In this figure, the solid curves indicate the computed density across the quartz chimney with the same discontinuity shown at $r/r_0 = 0$. For axisymmetric flow, ds/dr is zero. Therefore, to eliminate the density discontinuity, the left and right sides of the S -curve were averaged. The dashed curve in Figure 5-9 is the result of S -curve averaging. Figure 5-10 shows the actual fringe shift and the average fringe shift for interferogram 5-6.

The temperature ratio T_∞/T is just the inverse density ratio ρ/ρ_∞ since the molecular weights are nearly the same. The centerline temperature ratios for these two interferograms appear far too low, $T/T_\infty \lesssim 2$. This problem was discussed earlier in Section 4 and will be given further treatment later on in this section.

For the density calculations up to this point it was assumed that stoichiometric conditions exist. (See Section 4.8 and Figures 4-1 and 4-2). To show what effect the amount of excess air has on the calculation

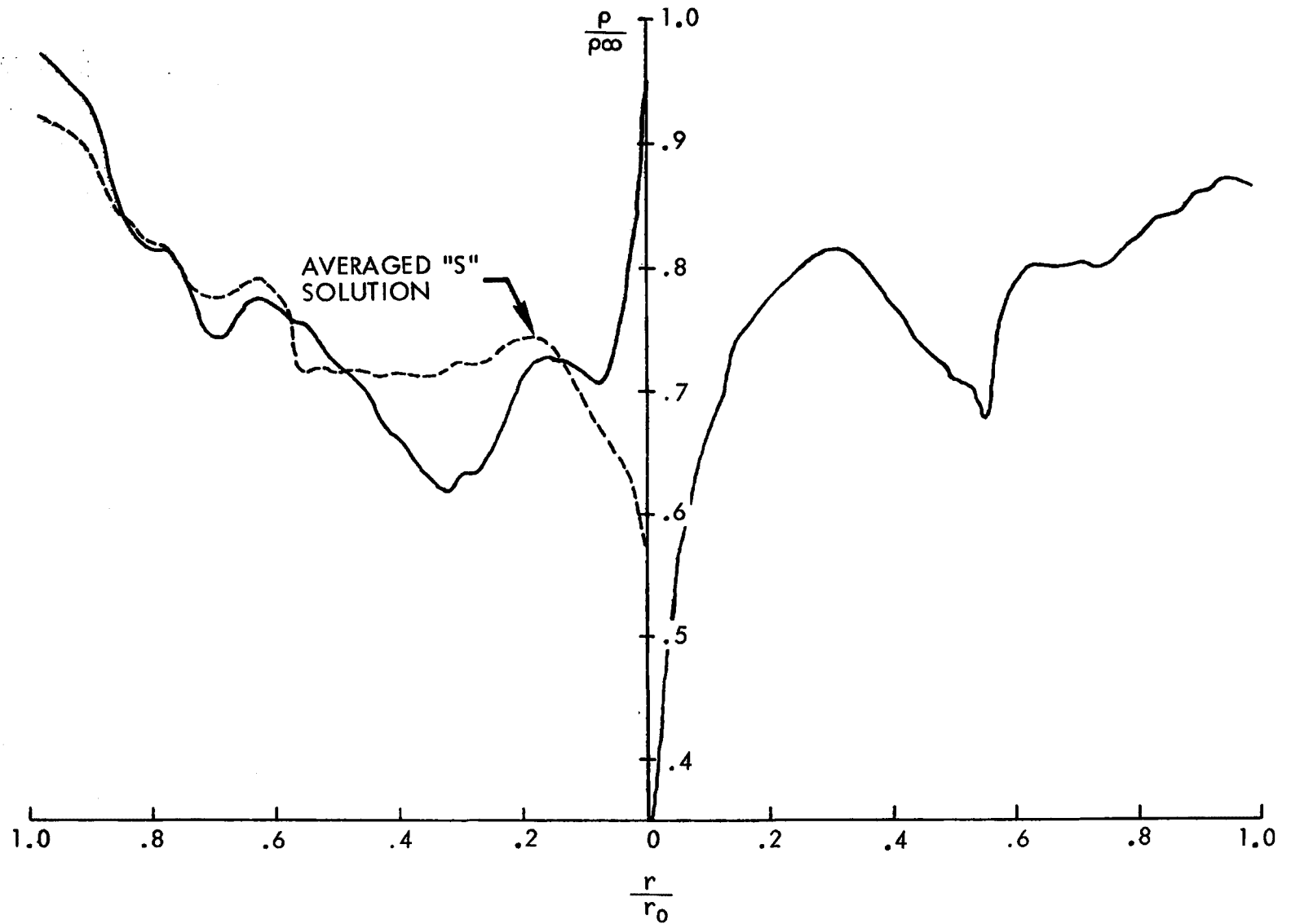


Figure 5-9. Density Solution for Interferogram EPA No. 5-6

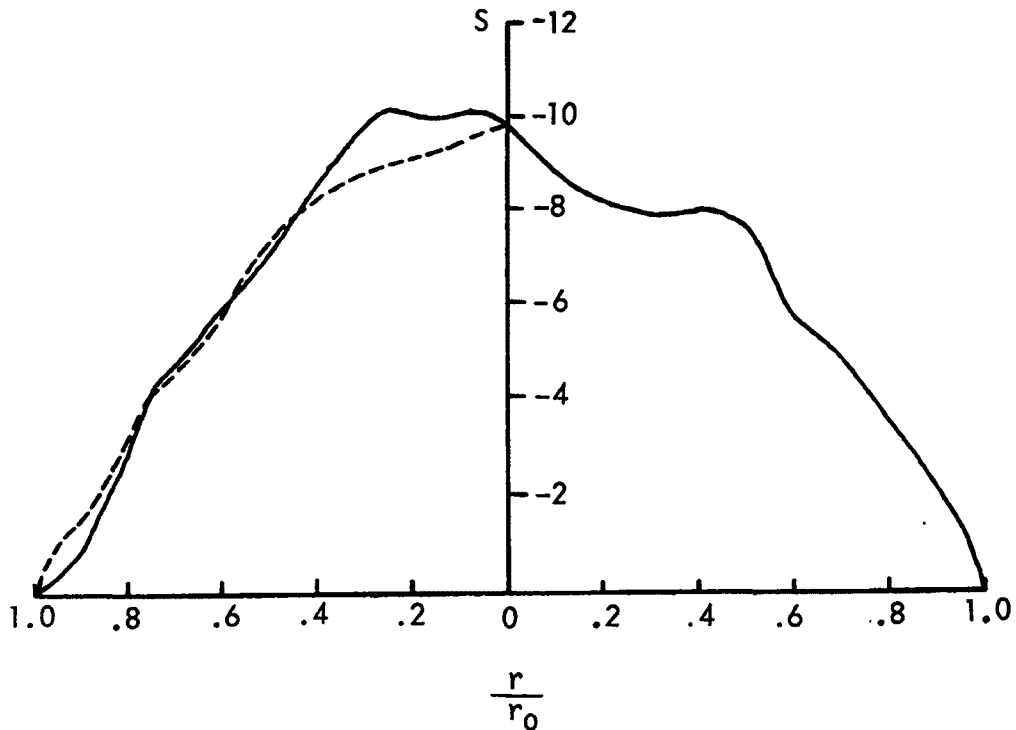


Figure 5-10. Fringe Shift for Interferogram EPA No. 5-6

of the density profile, a sample case was done using interferogram 5-6. The results are shown in Figure 5-11. The solid curve is the density profile as defined by stoichiometric conditions. The dashed curve is the density profile with an assumed 100 percent excess air (twice the amount of air needed for stoichiometric conditions). Allowing for the amount of excess air will lower the density for any one fringe shift profile.

In Figures 5-1 and 5-2, about 50 percent scene within the Pyrex chimney region is occluded and, therefore, it is impossible to make any determinable conclusion about the fringe shift profile in the occluded portion of the chimney. The Pyrex chimney has a wall thickness of 2.5 millimeter. By replacing this chimney with a fused quartz chimney with a wall thickness of 1.5 millimeter, the occluded regions were sufficiently decreased even though some waviness in the wall is observed. The result of this change decreased the occlusion to about 10 to 20 percent.

Since the quartz chimney also produced some occlusion, it was decided to use a rectangular box with Pyrex windows, used on an earlier EPA program, to circumvent the occluded areas produced by the edge of the round quartz chimney. An adapter was designed and fabricated to permit the

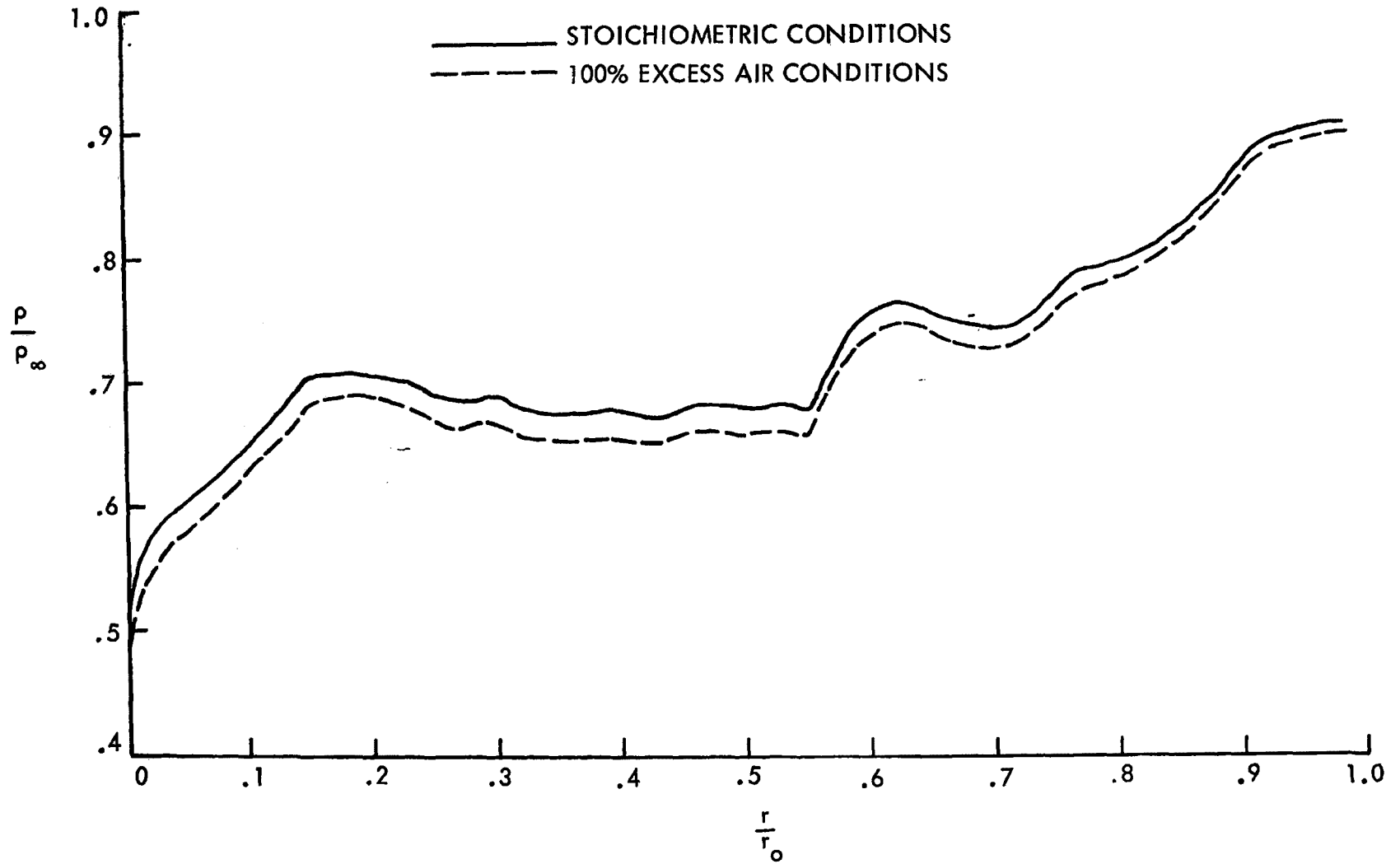


Figure 5-11. Effect of Excess Air on Density Profiles for Interferogram No. 5-6

mounting of the glass sealed box around the methane-air burner. Figure 5-12 shows an interferogram recorded with this configuration. The chief problem encountered with this approach is that the flame has a tendency to "wander" about inside the box, a characteristic which is not conducive in providing axisymmetric phenomena. For this reason, the rectangular box approach was abandoned.

It was noted earlier that data reduction procedures up to this point produce centerline temperatures which were too low. Referring to the modification in Section 4.4, a sample calculation was made using the data recorded in interferogram 5-6 to illustrate the feasibility of this procedure. It was assumed that the wall temperature was $T_w/T_\infty = 2^*$ and that stoichiometric combustion occurred.

A comparison between previous methods and this approach is shown in Figure 5-13. The centerline temperature is now calculated to be $T/T_\infty \approx 5.$, which is in a more probable temperature range.

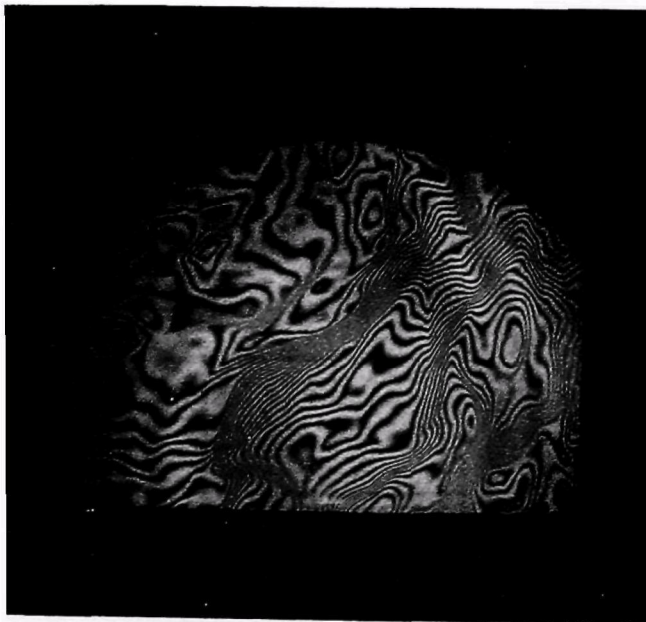


Figure 5-12. Test Interferogram for Rectangular Box with Pyrex Windows

* Thermocouple data support this value.

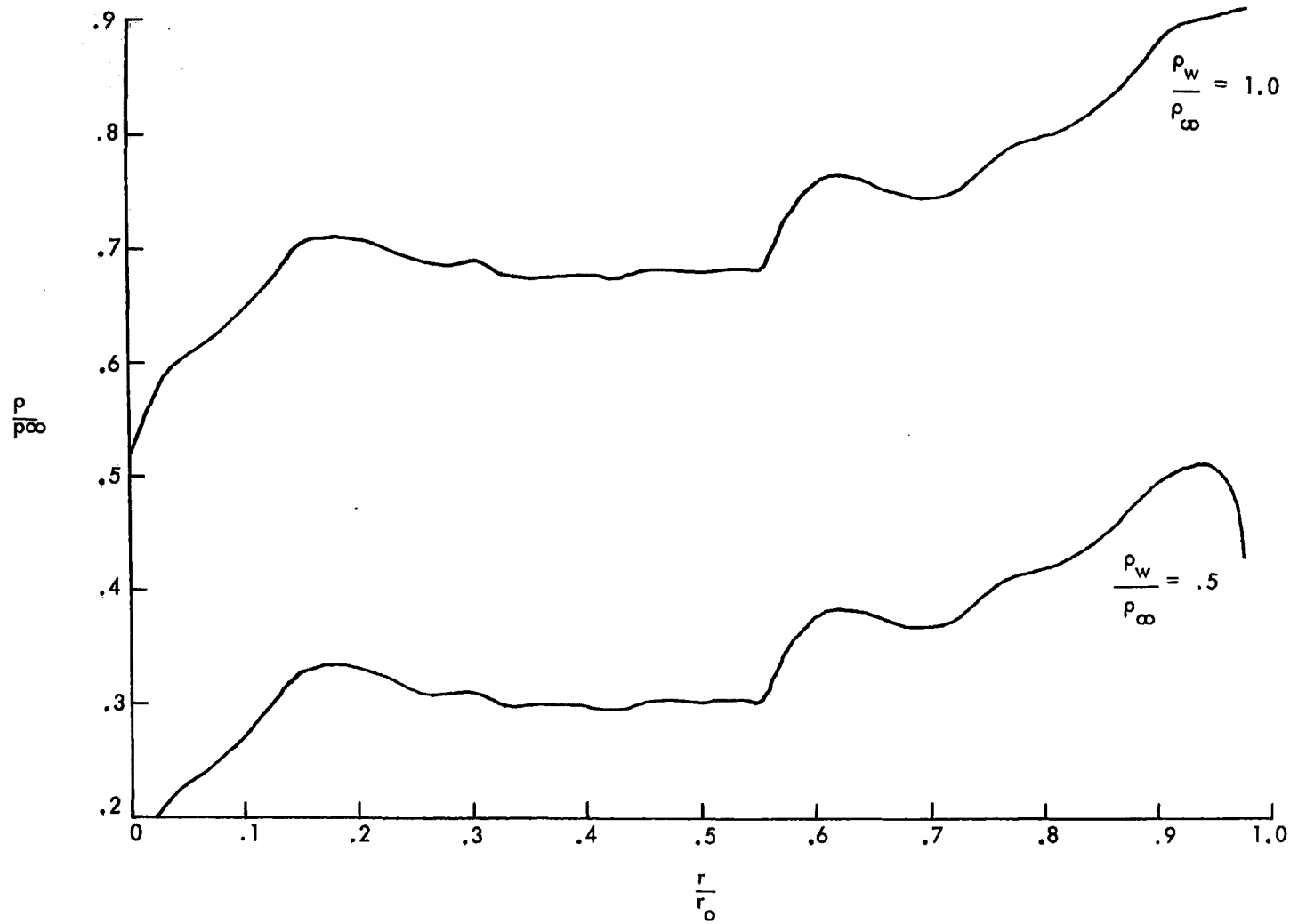


Figure 5-13. Effect of Wall Temperature on Density Profile for Interferogram No. 5-6

To apply the data reduction method above, chimney wall and gas centerline thermocouples were installed. The two wall thermocouples were of copper-constantan type. The thermocouples were bonded with sauerisen to each side of the fused quartz chimney at the scene centerline. The wall temperature was measured to be 456°F. The fused quartz chimney centerline thermocouple was of a chromel-alumel type. The gas centerline temperature was measured to be 1670°F. The air and methane were measured as 49870 cc/min and 4578 cc/min, respectively.

Two interferograms were taken at the same test conditions as were reported above. Also, additional thermocouple readings were recorded to insure repeatability of the initial test. These readings were well within 1 percent of the original readings. Figure 5-14 shows one of the interferograms recorded and used for data reduction purposes. All three thermocouples can be seen in this interferogram.

In order to validate the temperature calculated by the fringe shift recorded on the interferograms, comparisons were made to the gas temperature readings that were recorded from the thermocouple measurements and those computed from a theoretical adiabatic flame temperature calculation for a premixed methane-air flame. The method used included the dissociation of the combustion products over a range in percentage of excess air. This

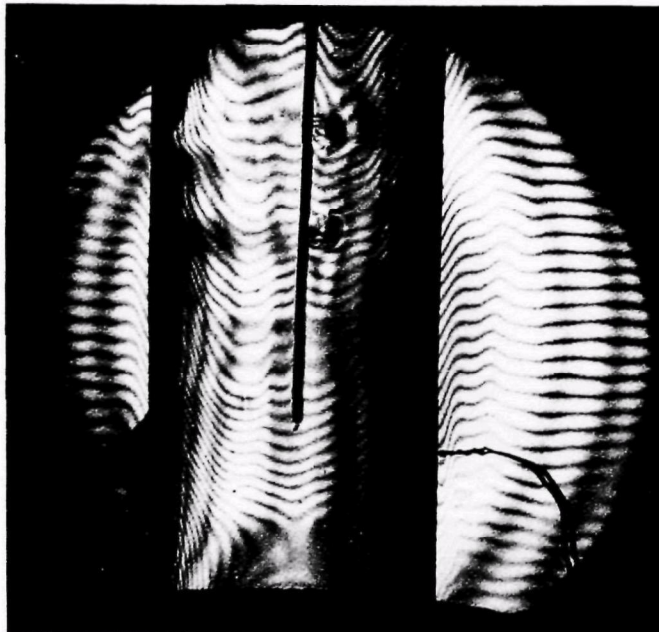


Figure 5-14. Interferogram with Thermocouples Attached

method is described in a book entitled "Flames" by A. G. Gaydon and H. G. Wolfhard.⁵ The results of this computer program are shown in Figures 5-15 and 5-16. In Figure 5-15, the temperature decreases as the percentage of excess air is increased from stoichiometric conditions (zero percent excess air) to 300 percent excess air. In Figure 5-16, the various combustion products are shown in terms of their individual partial pressures and how they are related to the percentage of excess air. Both the temperature and partial pressure of the combustion products have been verified at stoichiometric conditions.⁶ In Figure 5-17, the density profile for interferogram 5-14 is shown. The results of the measured fringe shift from this interferogram indicates a centerline temperature of 1777°F, which is much lower than the theoretical temperature at the indicated value of 14 percent excess air for this case. However, the fringe shift calculation of temperature is higher by 6 percent than the recorded thermocouple readings which are expected to be low because neither radiation nor heat condition loss corrections were made. The differences between the theoretical temperature and those of the fringe shift calculations and the thermocouple temperature reading may be caused by heat loss to the surroundings since the measurements were taken 3 inches above the actual burning surfaces.

5.5 DIFFUSION METHANE-AIR FLAME

Since a turbulent flame could not be produced in the premixed configuration, diffusion flames were studied to: (1) discover if a turbulent flame could be produced and a data reduction scheme provided for it, and (2) determine what effect, if any, fuel injection radius and air annulus radii would have on the temperature profiles.

In the study of effect of annulus radius, two annuli of different radii were used. The choice of annulus radii was somewhat arbitrary. However, to make a comparison of the effect that the annulus radius has on temperature profiles a significant difference in radius should be used. Thus, the inner annulus radii were selected to be 0.825 and 0.4 inch. Interferograms were taken at five different velocity ratios obtained by varying the amount of excess air at a given fuel rate. The range of excess air provided by the larger annulus radius is from 0 to 300 percent. Also, it was attempted to vary the Reynolds number by two orders of magnitude.

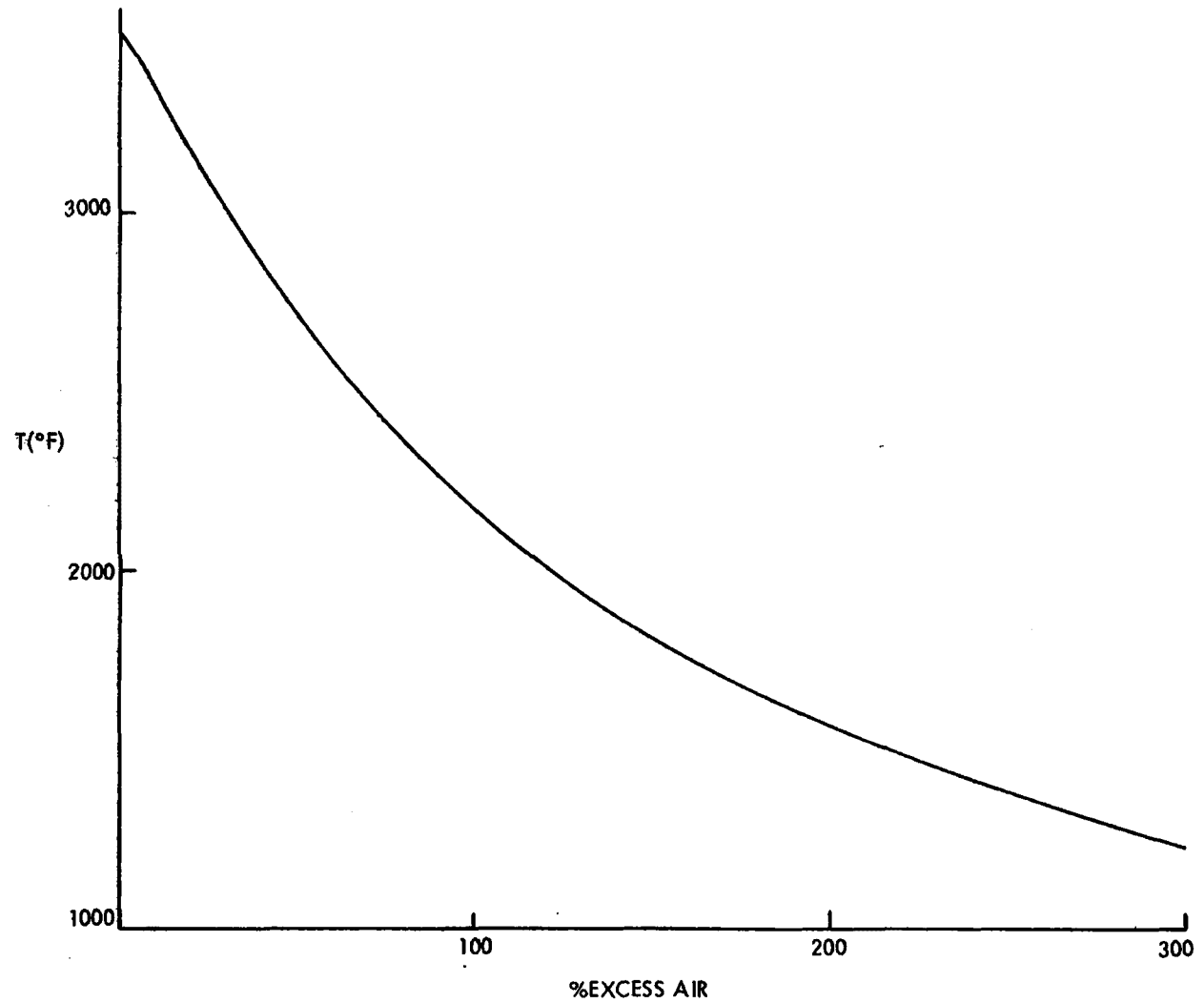


Figure 5-15. Temperature of Methane Air Premixed Flame Versus Percent Excess Air
Assumed: Dissociation of combustion products and no losses due to radiation, conduction nor convection)

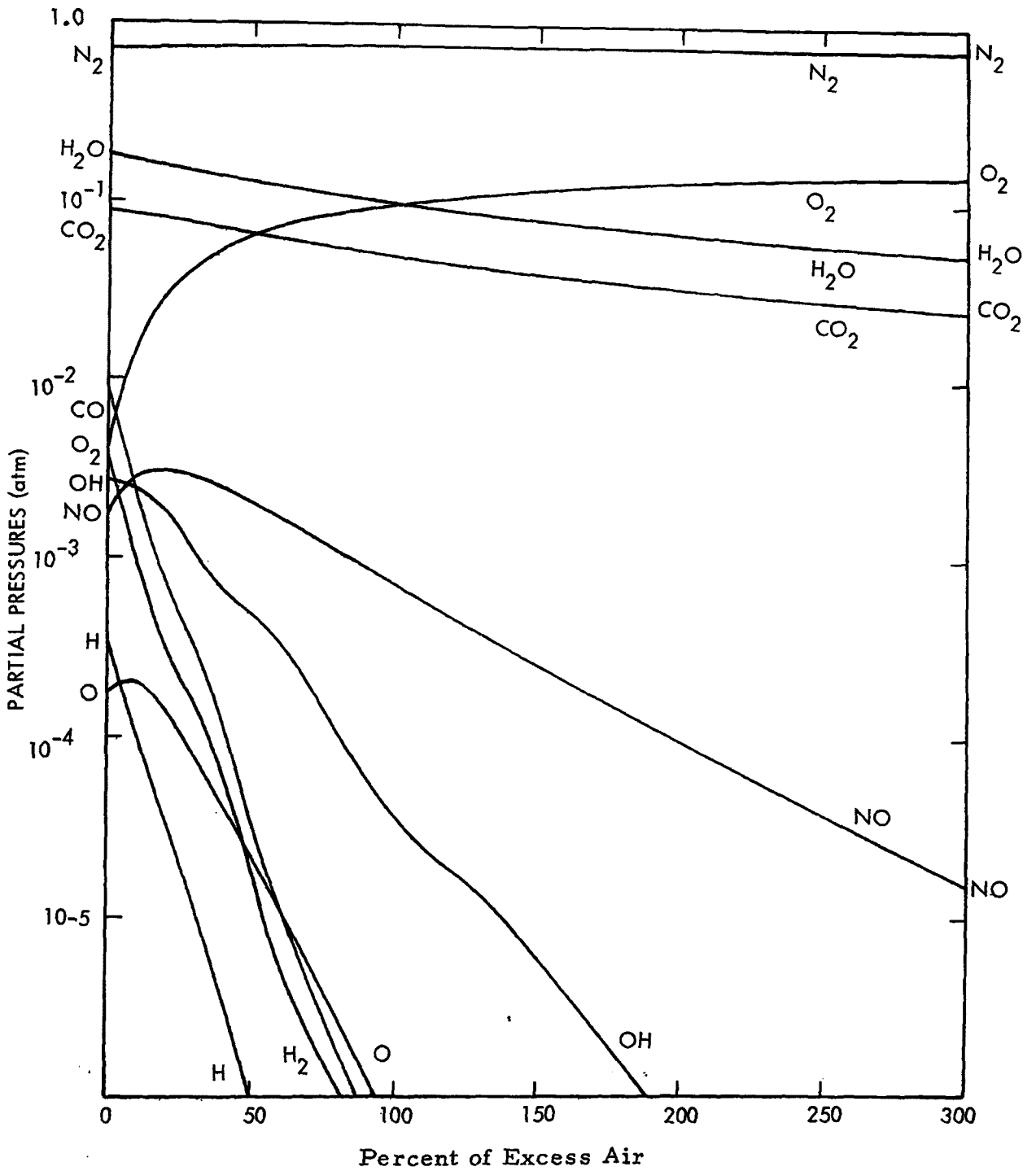


Figure 5-16. Partial Pressures of Combustion Products

Then, using the smaller annulus, a comparison series of tests was conducted. The flow rates for this series of tests were taken such that the velocity ratios remained the same, and the velocities of the individual gases were also the same between the two test series. However, the range of excess air was altered as dictated by the velocity requirements stated above.

In order to maintain the same velocities between these series of tests, the volumetric flow rates for each gas were adjusted according to the following:

$$Q_2 = \frac{Q_1}{A_1} A_2$$

where subscripts 1 and 2 refer to test series 1 and 2, respectively, and where Q is the flow rate and A is the area. By expressing this relationship in terms of the respective radii, one obtains for each gas,

$$Q_2 = Q_1 \frac{\pi(R^2 - r_2^2)}{\pi(R^2 - r_1^2)} \text{ (Air)}$$

and

$$Q_2 = Q_1 \frac{\pi r_2^2}{\pi r_1^2} \text{ (Methane)}$$

Therefore, when using the smaller inner radius ($r_2 = 0.4$) for the second test series, the air flow rate was increased by a factor of 1.39, and the methane flow rate was decreased by a factor of 4.25. This considerably increased the range of excess air from 489 to 2260 percent for the second series of tests. The test conditions are shown in Tables 5-2 and 5-3. These tables also include wall thermocouple temperature results and some visual flame descriptions.

Table 5-2. Test Conditions for Diffusion Flame with Radius of Annulus Equal to 0.825 Inch

Reynolds No. Factor	% Excess Air	Flow Rate (cc/min)		Velocity Ratio u_a/u_f	$\frac{Re}{L}$	$\frac{T_w}{T_\infty}$	Remarks
		Air	Methane				
1	0	945	99.1	3.15	158	1.20	} No burning Very small unstable flames
	50	1,420		4.72			
	100	1,830		6.29			
	200	2,840		9.45			
	300	3,700		12.58			
2	0	9,450	991.0	3.15	483	1.25	Smooth flame surface. Flame seems to collapse to a diameter less than inner annulus radius.
	50	14,200		4.72	662	1.21	
	100	18,900		6.29	845	1.20	
	200	28,400		9.45	1,210	1.19	
	300	37,800		12.58	1,580	1.18	
3	0	94,500	9910.0	3.15	4,330	1.35	Smooth flame, stable. Flame increases in length as amount of excess air increases.
	50	142,000		4.72	6,620	1.34	
	100	189,000		6.29	8,450	1.30	
	200	284,000		9.45	12,100	1.30	
	300	378,000		12.58	15,800	1.37	

Table 5-3. Test Conditions for Diffusion Flame with Inner Radius of Annulus Equal to 0.4 Inch.

Reynolds No. Factor	% Excess Air	Flow Rate (cc/min)		Velocity Ratio u_a/u_f	$\frac{Re}{L}$	$\frac{T_w}{T_\infty}$	Remarks
		Air	Methane				
1	489	1,310	23.3	3.15			} No burning
	786	1,970		4.72			
	1,080	2,630		6.29			
	1,690	3,950		9.45			
	2,260	5,250		12.58			
2	489	13,100	233.0	3.15	483	1.14	Small flame ~ 3 inches in length } Flame unstable 4 to 5 inches in length
	786	19,700		4.72	662	1.14	
	1,080	26,300		6.29	845	1.13	
	1,690	39,500		9.45	1,210	1.13	
	2,260	52,500		12.58	1,580	1.12	
3	489	131,000	2,330	3.15	4,330	1.16	Flame very long and losing smooth flame shape. Flame tends to shorten in length with increase of excess air. } Very turbulent flame
	786	197,000		4.72	6,620	1.17	
	1,080	263,000		6.29	8,450	1.17	
	1,690	395,000		9.45	12,100	1.17	
	2,260	525,000		12.58	15,800	1.13	

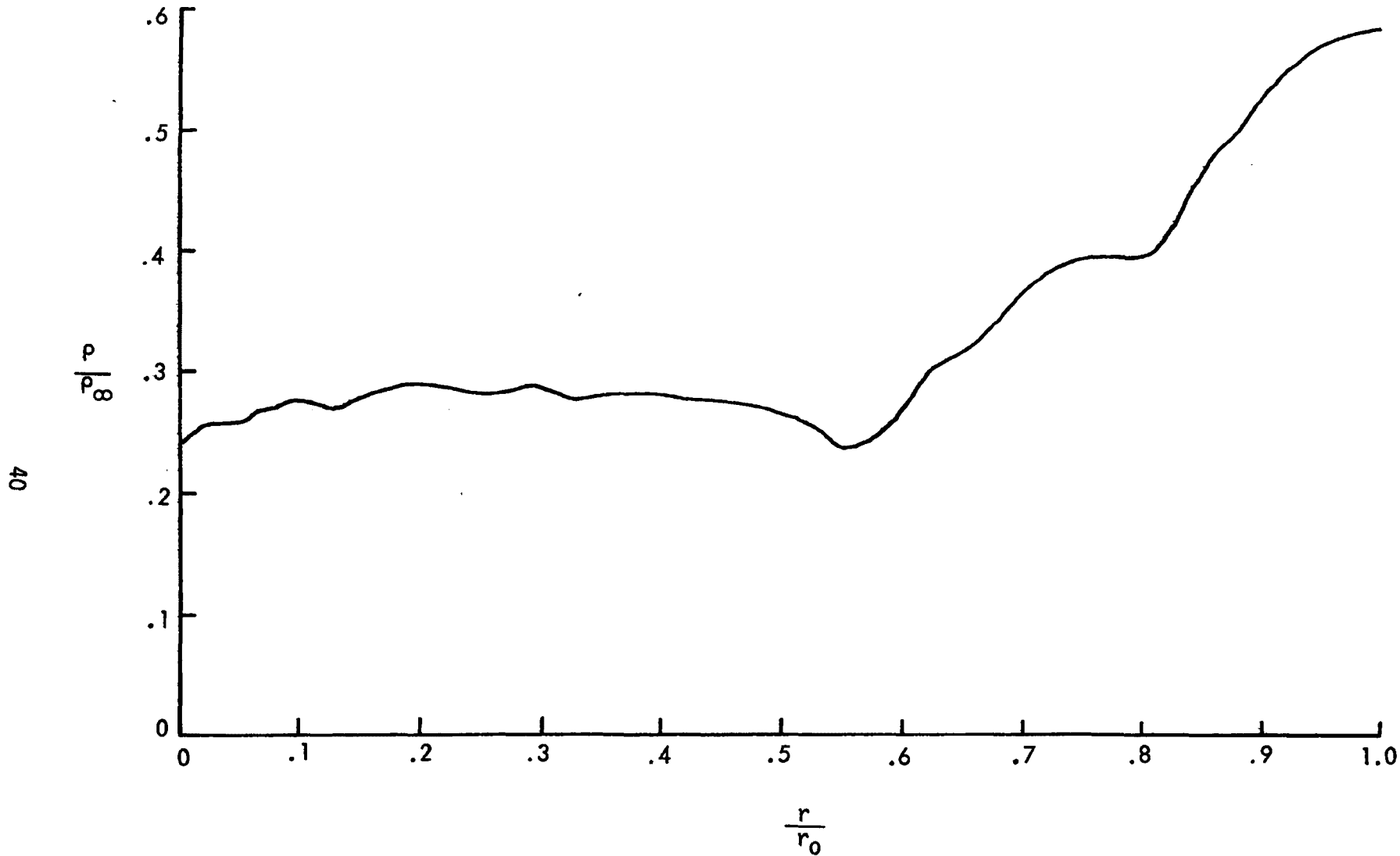


Figure 5-17. Density Profile for Interferogram No. 5-14 With 14 Percent Excess Air

For the interferogram data reduction procedure of the diffusion flame, the chimney cross section was divided into three regions (as shown in Figure 5-18):

- 1) The outer most region of the annulus was considered pure air.
- 2) The next region (moving towards the centerline) was identified as the stoichiometric combustion zone.
- 3) The centerline region was considered as pure unburned methane.

Using this description of zones in initial evaluation of temperature (results not shown), it was found that when the third region was assumed to be pure methane, very low temperatures at the centerline were computed ($T/T_{\infty} < 1$). Also, the temperature profile would markedly differ in the third region if the thickness of this region was varied. To explain further, the temperature would "drop" as the temperature profile passed through the second region to the third and, therefore, showed a dependency on the selected location of the boundary between these regions. This problem does not occur between the first and second region and was tested by shifting the location of their boundary.

Since the location of the third region boundary greatly influenced the temperature in the third region, it was not possible to define this region clearly. However, the location of the third region does not affect the calculation of the peak temperature in the temperature profile because the composition at the peak temperature is dominated by air and combustion products whose index and Gladstone-Dale relationships do not differ significantly. This problem cannot be solved using interferometry alone, but requires a separate measurement of gas composition.

Figures 5-19 through 5-29 are interferograms of the diffusion flame with $r = 0.825$ inch and with excess air, x , and velocity ratio, u_a/u_f as shown. The peak temperature, taken from the reduced temperature profile

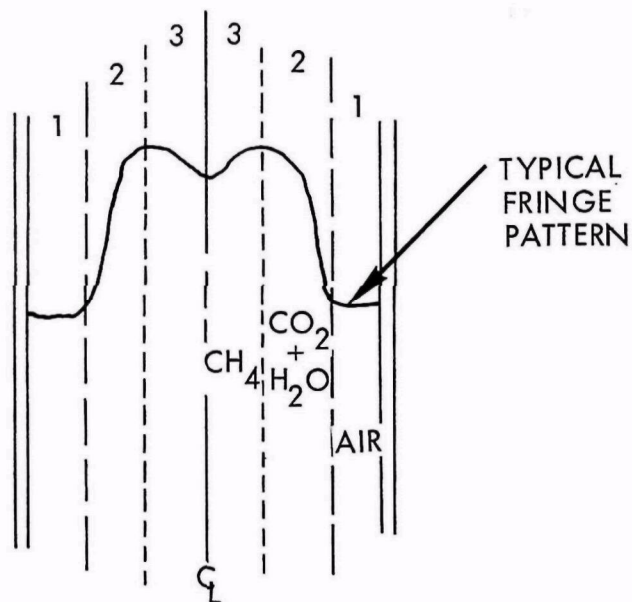


Figure 5-18. Schematic of Typical Fringe Pattern Divided Into Its Three Compositional Regions

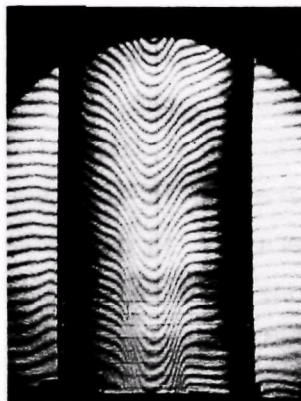


Figure 5-19

$$r = 0.825$$

$$\bar{u} = 0.0267$$

$$\frac{u_a}{u_f} = 12.58$$

$$x = 300\%$$

$$\frac{T}{T_\infty} = 3.13$$

Figure 5-19. Reconstructed Interferogram

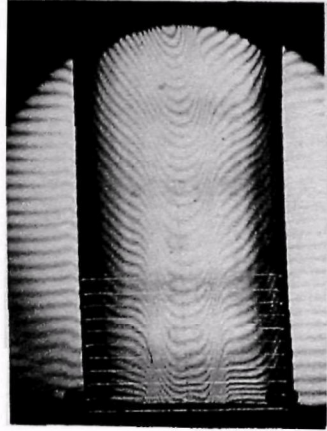


Figure 5-20

$$\begin{aligned} r &= 0.825 \\ \bar{u} &= 0.0817 \\ \frac{u_a}{u_f} &= 3.15 \\ x &= 0\% \\ \frac{T}{T_\infty} &= 2.89 \end{aligned}$$

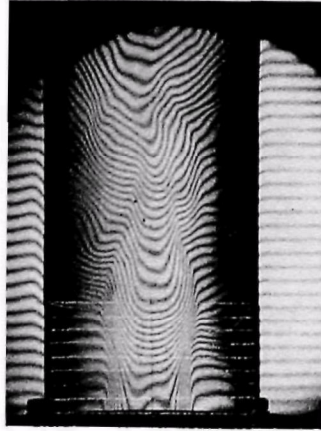


Figure 5-21

$$\begin{aligned} r &= 0.825 \\ \bar{u} &= 0.112 \\ \frac{u_a}{u_f} &= 4.72 \\ x &= 50\% \\ \frac{T}{T_\infty} &= 4.0 \end{aligned}$$

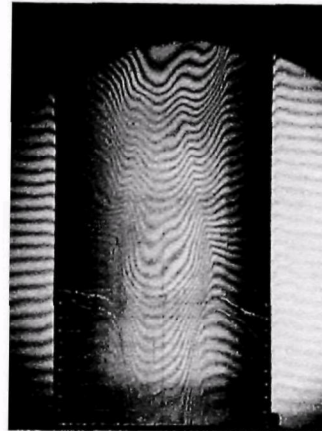


Figure 5-22

$$\begin{aligned} r &= 0.825 \\ \bar{u} &= 0.143 \\ \frac{u_a}{u_f} &= 6.29 \\ x &= 100\% \\ \frac{T}{T_\infty} &= 3.03 \end{aligned}$$

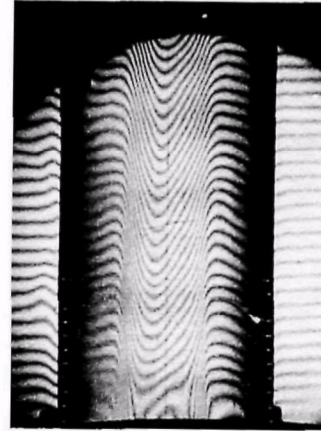


Figure 5-23

$$\begin{aligned} r &= 0.825 \\ \bar{u} &= 0.205 \\ \frac{u_a}{u_f} &= 9.45 \\ x &= 200\% \\ \frac{T}{T_\infty} &= 3.3 \end{aligned}$$

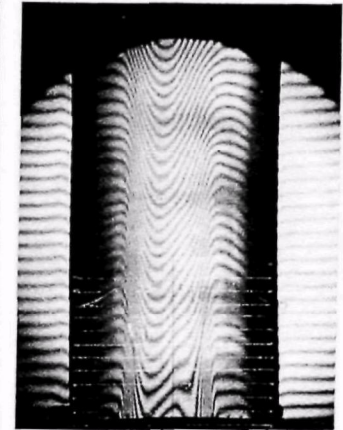


Figure 5-24

$$\begin{aligned} r &= 0.825 \\ \bar{u} &= 0.267 \\ \frac{u_a}{u_f} &= 12.58 \\ x &= 300\% \\ \frac{T}{T_\infty} &= 4.0 \end{aligned}$$

Figures 5-20 through 5-24. Reconstructed Interferograms

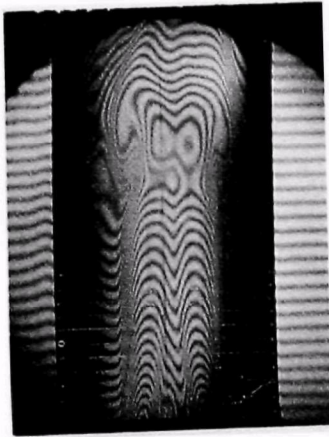


Figure 5-25

$$\begin{aligned} r &= 0.825 \\ \bar{u} &= 0.817 \\ \frac{u_a}{u_f} &= 3.15 \\ x &= 0\% \\ \frac{T}{T_\infty} &= 4.30 \end{aligned}$$

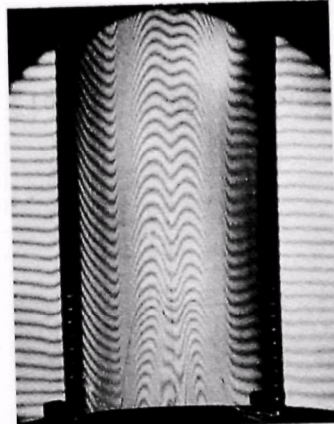


Figure 5-26

$$\begin{aligned} r &= 0.825 \\ \bar{u} &= 0.817 \\ \frac{u_a}{u_f} &= 4.72 \\ x &= 50\% \\ \frac{T}{T_\infty} &= 3.65 \end{aligned}$$

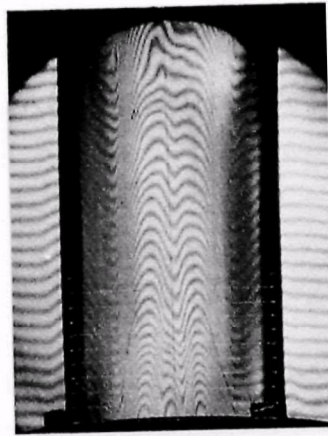


Figure 5-27

$$\begin{aligned} r &= 0.825 \\ \bar{u} &= 1.12 \\ \frac{u_a}{u_f} &= 6.29 \\ x &= 100\% \\ \frac{T}{T_\infty} &= 3.97 \end{aligned}$$

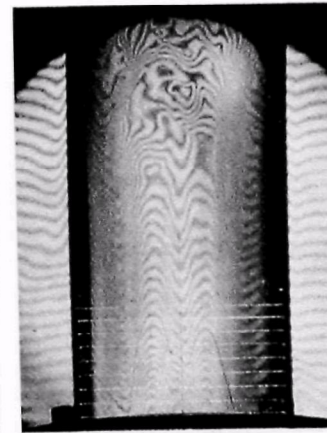


Figure 5-28

$$\begin{aligned} r &= 0.825 \\ \bar{u} &= 1.43 \\ \frac{u_a}{u_f} &= 9.45 \\ x &= 200\% \\ \frac{T}{T_\infty} &= 3.0 \end{aligned}$$

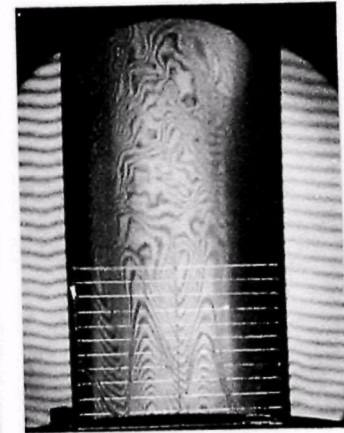


Figure 5-29

$$\begin{aligned} r &= 0.825 \\ \bar{u} &= 2.05 \\ \frac{u_a}{u_f} &= 12.58 \\ x &= 300\% \\ \frac{T}{T_\infty} &= 4.41 \end{aligned}$$

Figures 5-25 through 5-29. Reconstructed Interferograms

data, is also shown in the legend of each figure and is plotted later on. The sequence of photographs are in order of increasing Reynolds number. Fringe shift near the wall is minimal, indicating small changes in temperature. Proceeding inward towards the centerline, the abrupt fringe shift results from the lower density, higher temperature "flame sheet" occurring at the air-fuel interface. The trend with increasing Reynolds number which is directly proportional to

$$\bar{u} = \frac{u_a' + u_f}{2} = \frac{u_a}{2} \left[1 + \frac{1}{u_a/u_f} \right]$$

is that the flame width decreases, a result consistent with a laminar mixing-reaction zone. The interferometric data for $r = 0.4$ inch are shown in Figures 5-30 through 5-39 and exhibit the same trends as the data at $r = 0.825$ inch.

During some preliminary work conducted before actual interferometry on diffusion flames, thermocouple measurements were taken. The thermocouple was located about 0.25 inch above the burner surface and emerged at the edge of the visible flame front. This location was selected after some probing was done to find where the maximum temperature occurs. (It should be noted that when reducing the interferogram data, it was not always possible to select a fringe which corresponds to the thermocouple location.) The results of the thermocouple measurements indicate only a slight increase in temperature with increase of excess air. The phenomenon differs greatly with the findings of premixed flame configuration which indicated a substantial temperature dependence on the percentage of excess air.

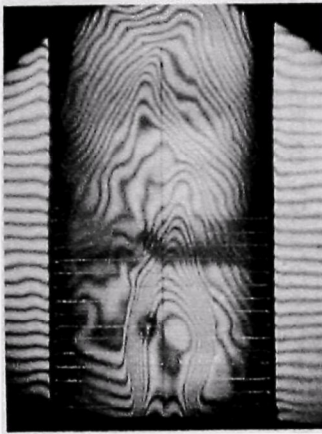


Figure 5-30

$$\begin{aligned} r &= 0.4 \\ \bar{u} &= 0.0817 \\ \frac{u_a}{u_f} &= 3.15 \\ x &= 489\% \\ \frac{T}{T_\infty} &= 5.5 \end{aligned}$$

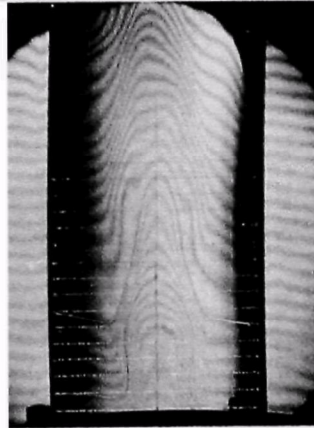


Figure 5-31

$$\begin{aligned} r &= 0.4 \\ \bar{u} &= 0.112 \\ \frac{u_a}{u_f} &= 4.72 \\ x &= 786\% \\ \frac{T}{T_\infty} &= 3.95 \end{aligned}$$

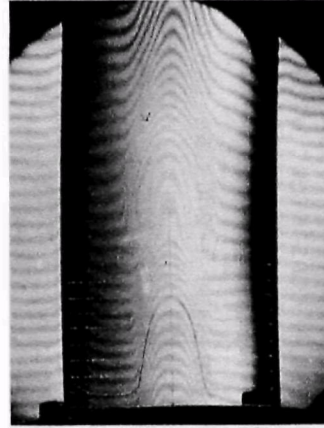


Figure 5-32

$$\begin{aligned} r &= 0.4 \\ \bar{u} &= 0.143 \\ \frac{u_a}{u_f} &= 6.29 \\ x &= 1080\% \\ \frac{T}{T_\infty} &= 4.17 \end{aligned}$$

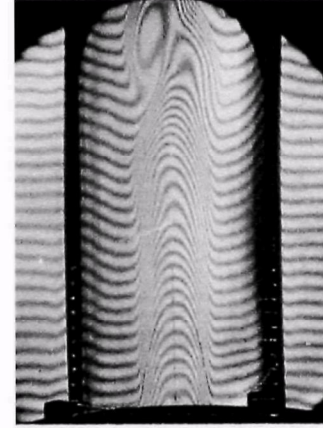


Figure 5-33

$$\begin{aligned} r &= 0.4 \\ \bar{u} &= 0.205 \\ \frac{u_a}{u_f} &= 9.45 \\ x &= 1680\% \\ \frac{T}{T_\infty} &= 3.33 \end{aligned}$$

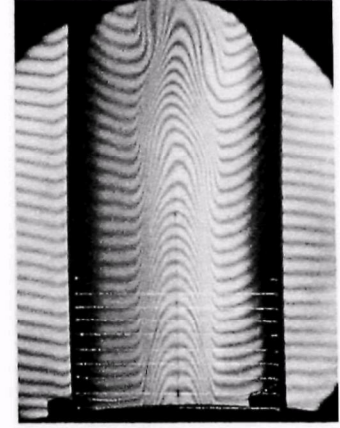


Figure 5-34

$$\begin{aligned} r &= 0.4 \\ \bar{u} &= 0.267 \\ \frac{u_a}{u_f} &= 12.58 \\ x &= 2260\% \\ \frac{T}{T_\infty} &= 3.33 \end{aligned}$$

Figures 5-30 through 5-34. Reconstructed Interferograms

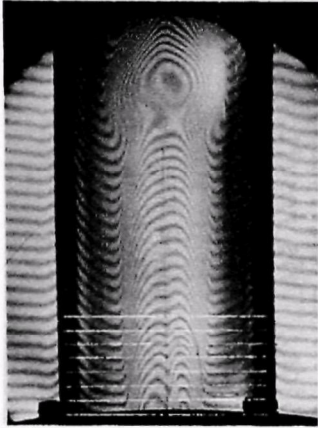


Figure 5-35

$$\begin{aligned}
 r &= 0.4 \\
 \bar{u} &= 0.817 \\
 \frac{u_a}{u_f} &= 3.15 \\
 x &= 489\% \\
 \frac{T}{T_\infty} &= 3.16
 \end{aligned}$$

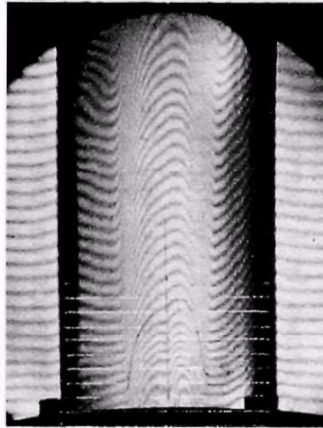


Figure 5-36

$$\begin{aligned}
 r &= 0.4 \\
 \bar{u} &= 1.12 \\
 \frac{u_a}{u_f} &= 4.72 \\
 x &= 786\% \\
 \frac{T}{T_\infty} &= 2.30
 \end{aligned}$$

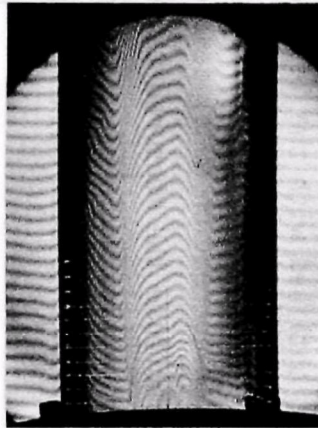


Figure 5-37

$$\begin{aligned}
 r &= 0.4 \\
 \bar{u} &= 1.43 \\
 \frac{u_a}{u_f} &= 6.29 \\
 x &= 1080\% \\
 \frac{T}{T_\infty} &= 2.40
 \end{aligned}$$

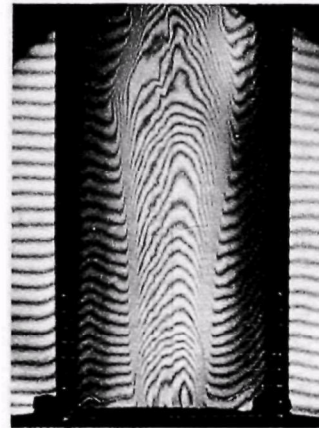


Figure 5-38

$$\begin{aligned}
 r &= 0.4 \\
 \bar{u} &= 2.05 \\
 \frac{u_a}{u_f} &= 9.45 \\
 x &= 1680\% \\
 \frac{T}{T_\infty} &= 3.10
 \end{aligned}$$

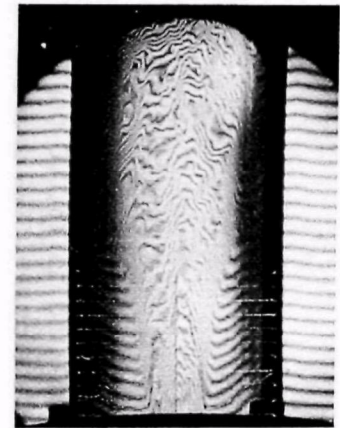


Figure 5-39

$$\begin{aligned}
 r &= 0.4 \\
 \bar{u} &= 2.67 \\
 \frac{u_a}{u_f} &= 12.58 \\
 x &= 2260\% \\
 \frac{T}{T_\infty} &= 4.68
 \end{aligned}$$

Figures 5-35 through 5-39. Reconstructed Interferograms

Figure 5-40 shows the peak temperature as a function of averaged streams' velocities, \bar{u} , which provides a Reynolds number per unit length range of two orders of magnitude, varying from ~ 160 to 16,000 per foot. The mean temperature appears to be about $T/T_\infty = 3.5$ or $T \cong 300 \times 3.5 = 1050^\circ\text{K}$ (1430°F). Disallowing the one high data point near $\bar{u} = 0.08$ ft/sec, variations of the data about the mean temperature increase with u or Re . This observation is consistent with the idea of an unstable laminar flame sheet in the transition region. Recall that at the highest Reynolds numbers the flame looks turbulent. See especially the highest Reynolds number interferogram data at $r = 0.4$.

The solid curve in the intermediate range of \bar{u} represents flame thermocouple measurements. Good agreement is obtained with the interferometric data. No corrections were made to the thermocouple measurements for radiation losses. By using the radiation correction model developed on the earlier EPA contract, a correction to increase the measured temperature by about 20 percent is indicated. This correction would place the measurements very near the upper range of the interferometric data rather than at the average.

Local temperature profile data are shown in Figures 5-41, 5-42 and 5-43 at $r = 0.825$ inch and Figures 5-44 and 5-45 at $r = 0.4$ inch. Shown in the legend are also the values of excess air, x , velocity ratio u_a/u_f , and average velocity, \bar{u} . Examination of these data reveal the following trends:

- a) Strong \bar{u} (Reynolds number) dependence on the peak temperature location is observed for constant u_a/u_f and x for a 10^2 range in Reynolds number. As Re increases, the flame sheet moves towards the air side. This result is indicative of what might be expected of a turbulent flame or a "transitional" flame (Figure 5-41).
- b) For each r value of the annulus (compare Figures 5-42 and 5-43 and 5-44 and 5-45), this same effect is observed independent of velocity ratio of excess air.

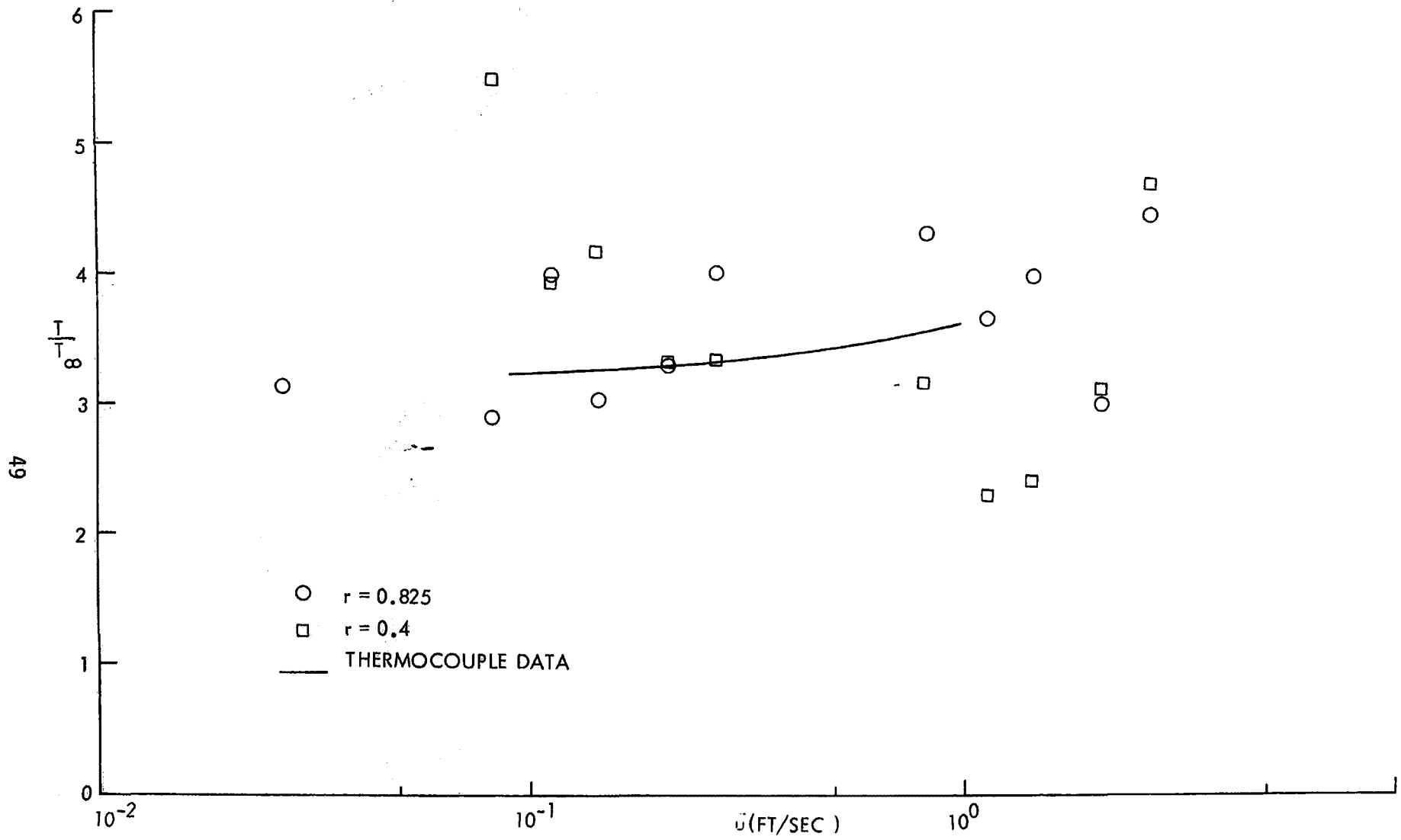


Figure 5-40. Plot of Peak Temperatures of Reduced Interferograms and Thermocouple Data

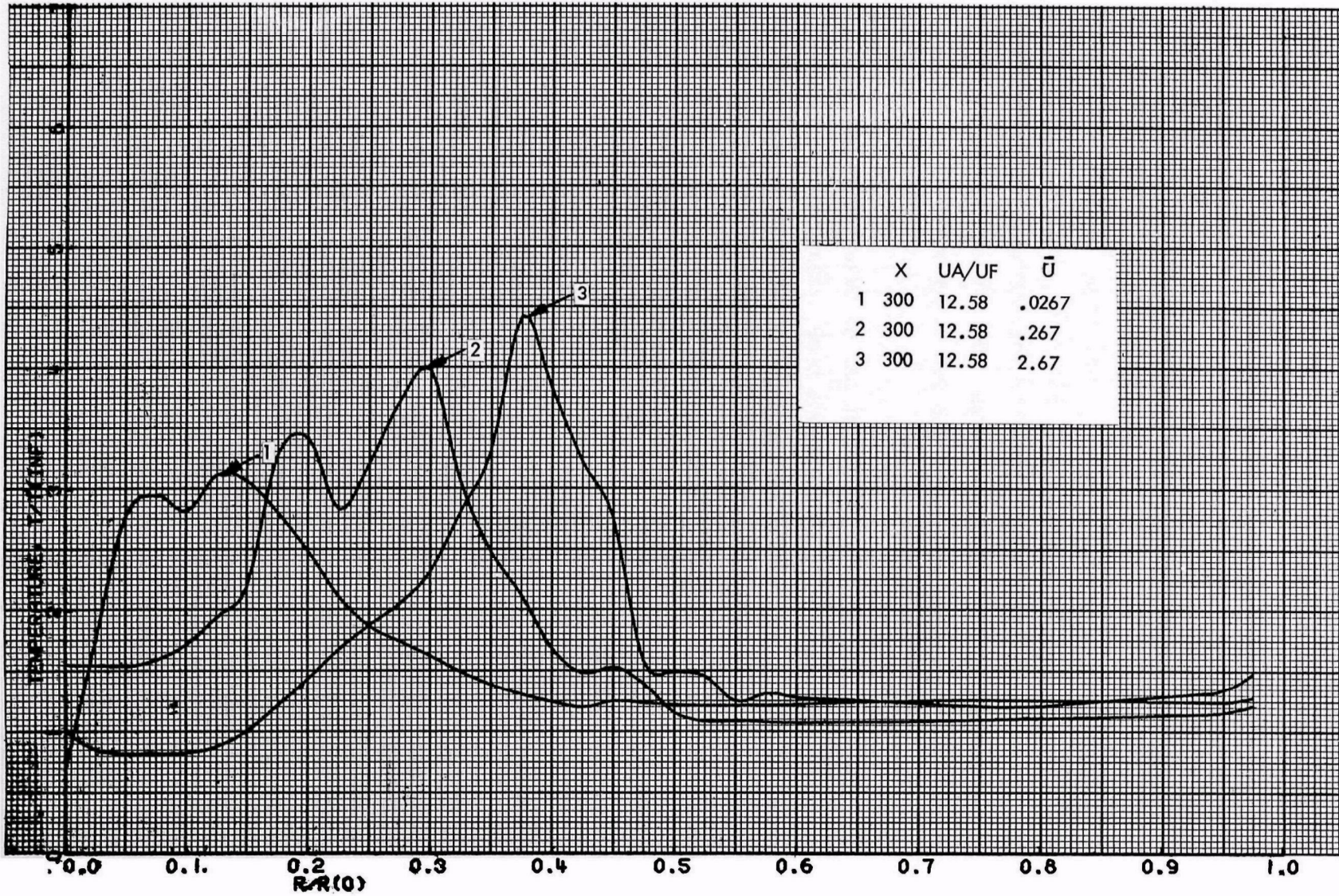


Figure 5-41. Temperature Profiles With $r = 0.825$ inch, Varying Reynolds Number, Constant UA/UF

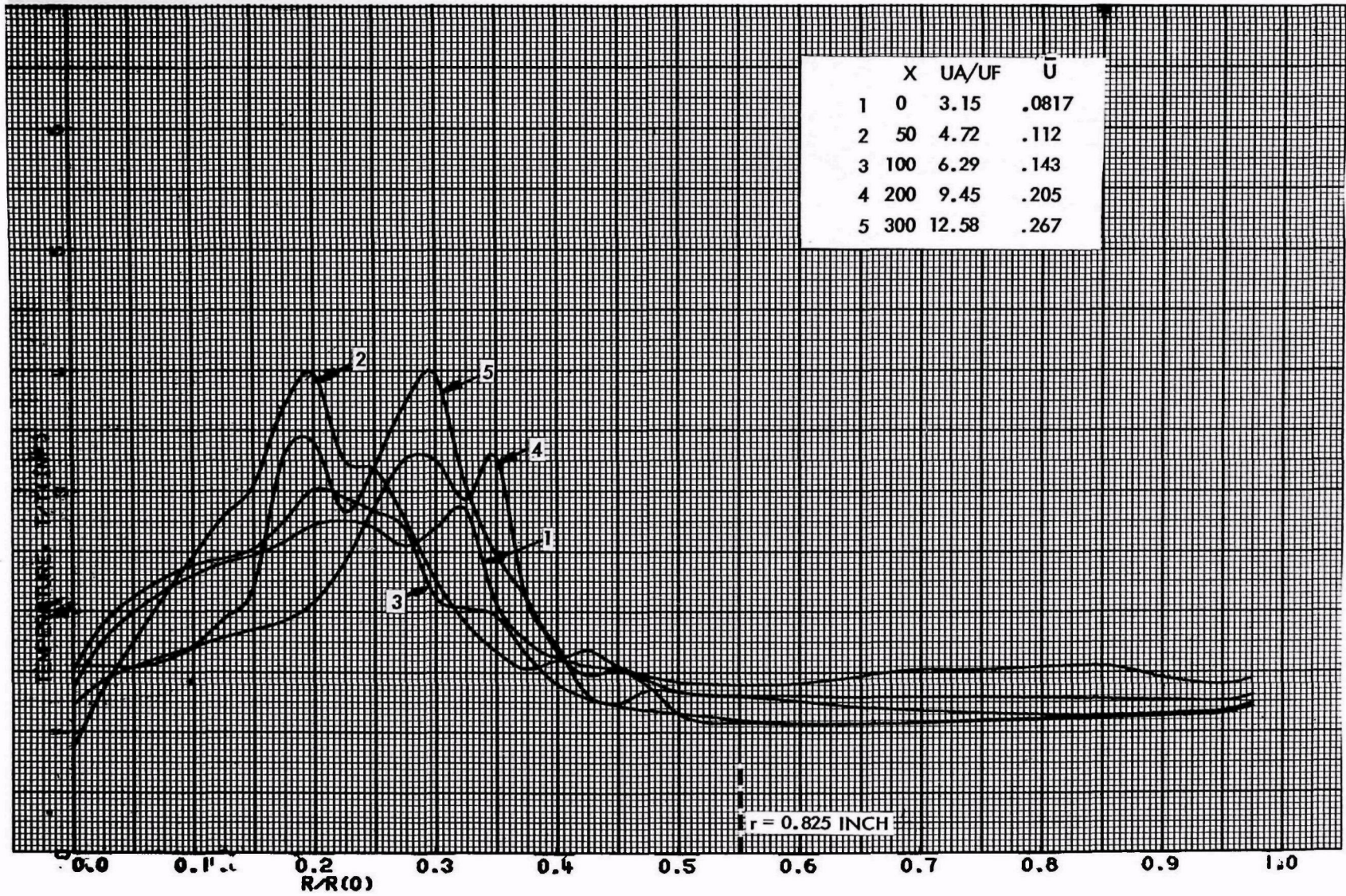


Figure 5-42. Temperature Profiles With $r = 0.825$ inch, Medium Reynolds Number, Varying UA/UF

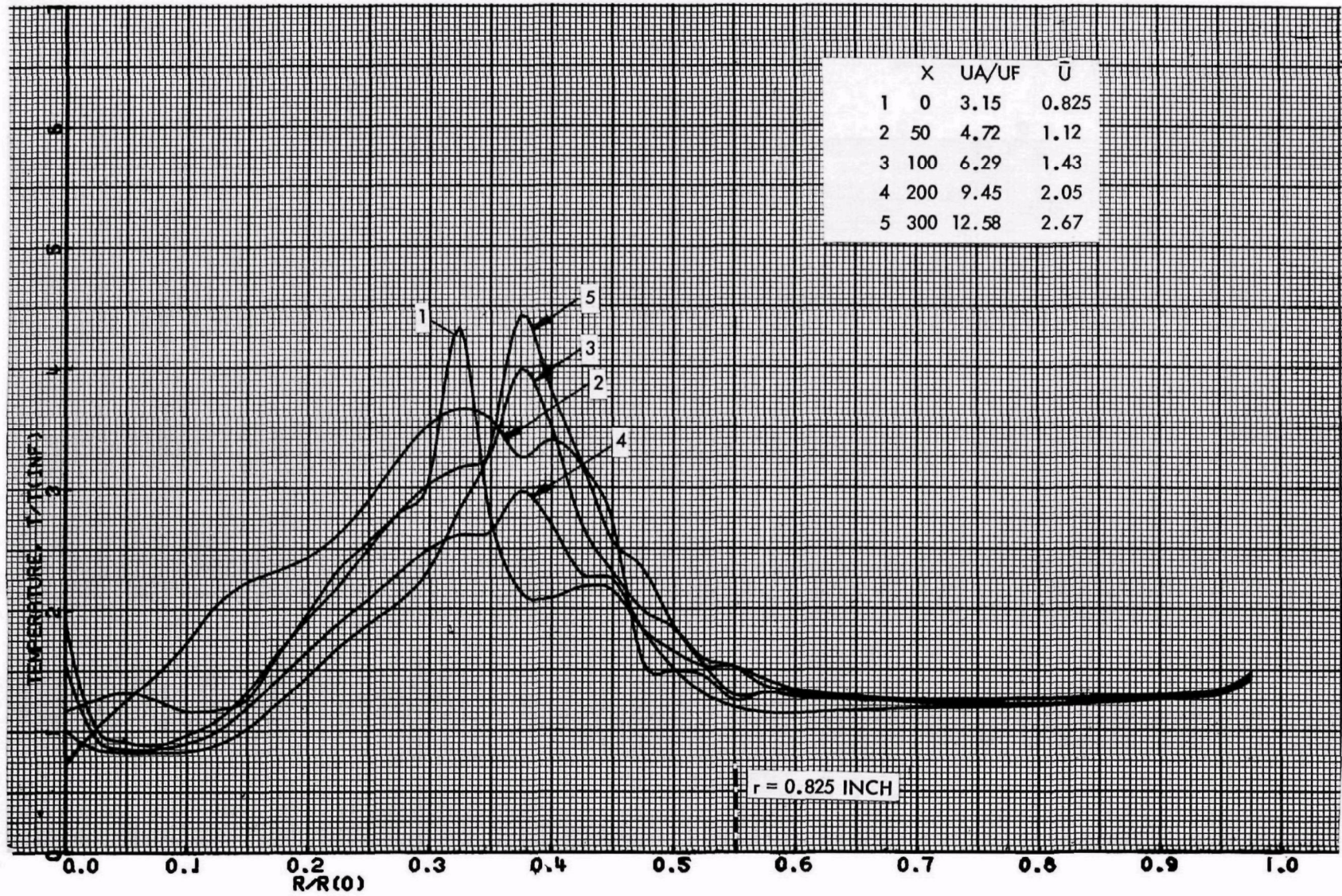


Figure 5-43. Temperature Profiles With $r = 0.825$ inch, High Reynolds Number Varying UA/UF

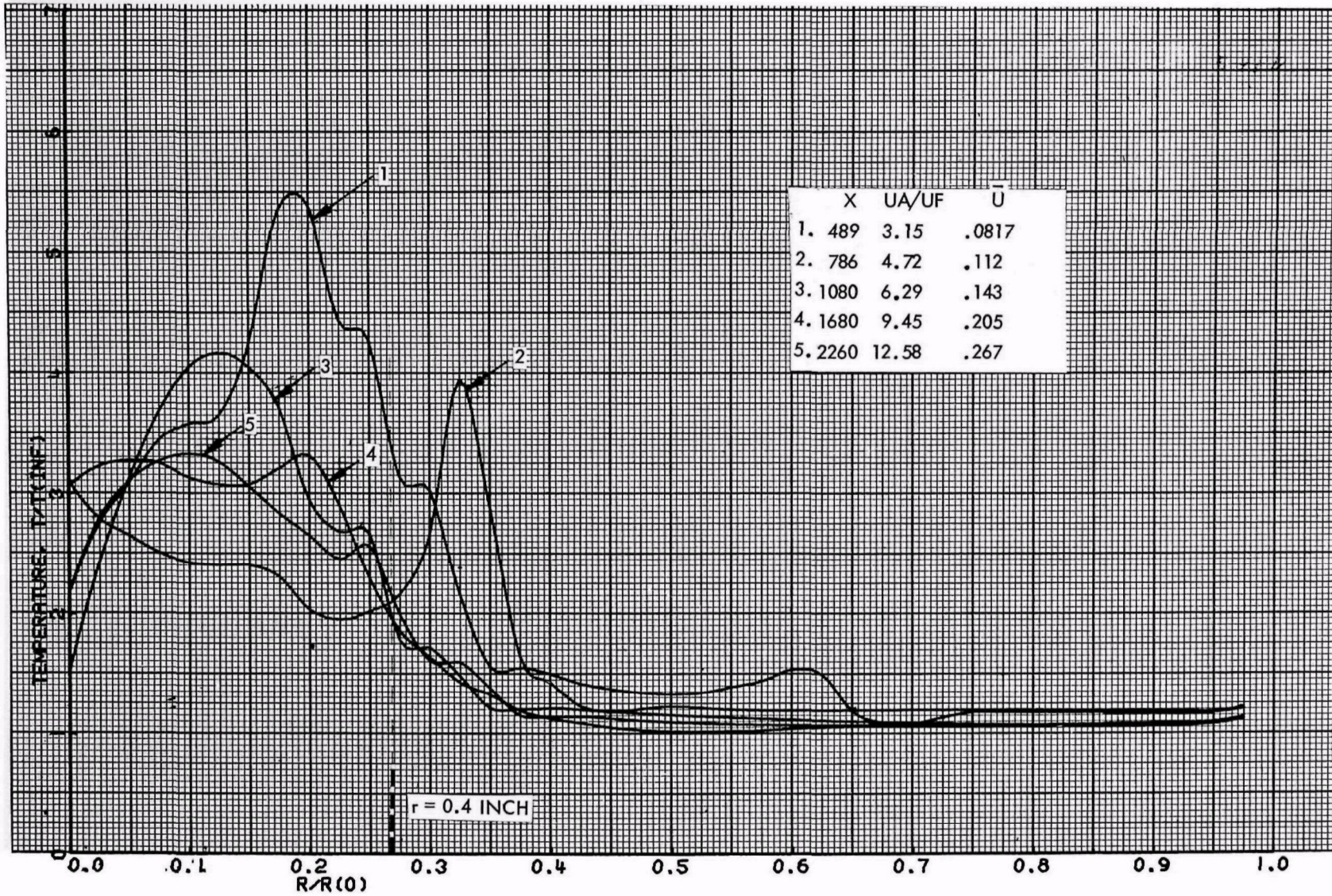


Figure 5-44. Temperature Profiles With $r = 0.4$ inch, Medium Reynolds Number, Varying UA/UF

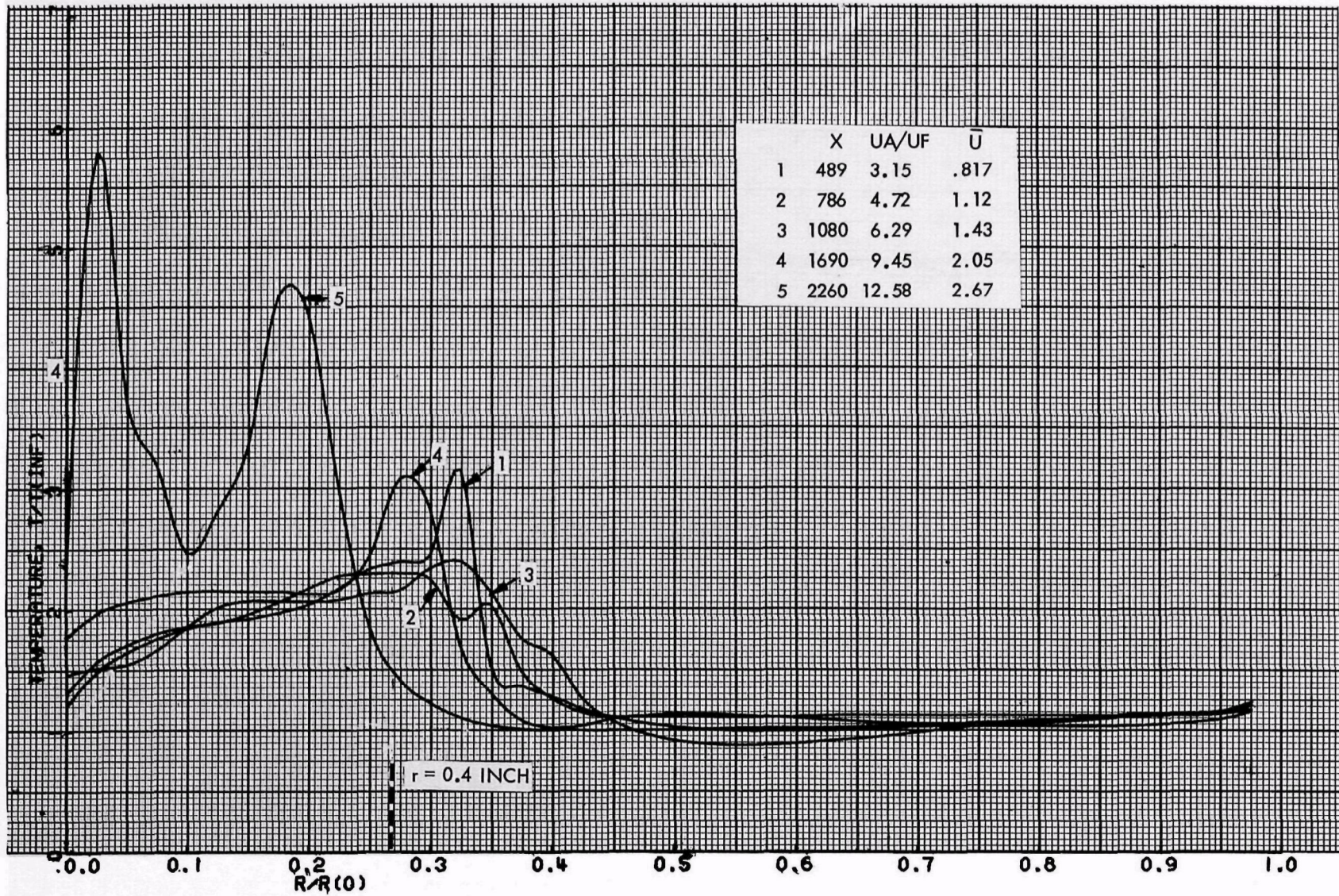


Figure 5-45. Temperature Profiles With $r = 0.4$ inch, High Reynolds Number, Varying UA/UF

- c) For a given Re , considerable variation in position of peak temperature signal is present. This is believed to be caused by the fluctuating or transitional character of the flame zone.
- d) No clear difference exists between the $r = 0.4$ and 0.825 inch cases.

6. CONCLUSIONS AND RECOMMENDATIONS

6.1 CONCLUSIONS

6.1.1 Interferometric Data Reduction Procedures

- a) The basic equation for fringe shift was inverted to provide unique determination of the density field for the case of axisymmetric phenomena, which turned out to be a fairly good approximation in most cases. Modifications were included for differences in molecular weight and refractive index between the reference and test scenes of the burner.
- b) A data reduction model was developed which allowed the reduction of interferometric data when the chimney wall became hot. Basically, the procedure allowed the incorporation of a thermocouple wall temperature measurement which obviated the high fringe density and internal reflection present at the chimney wall for the premixed flame.
- c) It was shown by calculation that errors in knowledge of the composition for the premixed flame produced small errors in the final computed density and temperature field because the index, index-density, and density-temperature relationships were dominated by those properties of air, at least for those conditions investigated here for stoichiometric and excess air combustion.
- d) For the data reduction model developed for the diffusion flame, it was found that the air side of the flame could be computed somewhat independently of knowing what the actual species composition was in the diffusion layer whereas the features of the fuel side of the sheet were strongly dependent on the composition in the diffusion layer between the fuel and the flame sheet. Thus, the overall variation of index, index-density, and density-temperature across the flame is too large to expect an interferometric measurement alone to provide temperature, at least for the fuel side of the flame sheet.

6.1.2 Diffusion Flame

- a) The diffusion flame was operated over a Reynolds number range of 100. Reynolds number per unit length, $Re/L = u/\nu$, was varied by increasing both air and fuel flow rates and by increasing the air flow rate (increasing percent excess air) at fixed fuel rate.
- b) Variations about the peak temperatures calculated from these data increased as a function of Reynolds number. This phenomenon is believed to be caused by the increasing frequency of unstable spots (turbulent spots) in the flame sheet.

- c) Thermocouple data provided excellent agreement with mean of the interferometric data.
- d) The large range in Reynolds number investigated provided data for the diffusion (laminar) flame and at the highest two Reynolds number, data for the turbulent flame.

6.1.3 Premixed Flame

Largely because of the extensive work done to provide a suitable data reduction procedure for the case of the premixed flame, i.e., to account for the occluded region at the chimney wall, data were recorded and reduced at only one Reynolds number and one value of excess air. Good agreement was obtained between the thermocouple inserted in the flame and the interferometric data albeit the measurements were much lower than the adiabatic flame temperature.

6.1.4 Oil Burners

At present, holographic interferometry does not appear applicable to highly turbulent-complex-real flames (i.e., oil burners). However, laboratory flames that are in the transitional or slightly turbulent regime can be evaluated by this technique.

6.2 RECOMMENDATIONS

- a) Future studies should be conducted with a wrap-around 180-degree viewing-angle holographic interferometer to provide adequate three-dimensional coverage so as to allow accurate measurement of strongly asymmetric flames caused by either or both turbulence or asymmetric burner configurations.
- b) Diffusion flame cannot be analyzed quantitatively by interferometry alone. A mass composition probe is necessary to provide data on the fuel-side diffusion zone of the flame sheet. It does not appear that a complicated non-equilibrium sampling procedure is justified since the index of the non-equilibrium products properly averaged may be equal to the equilibrium value. Thus, a simple aspirating probe may be adequate.
- c) It is strongly recommended that the feasibility of chemiluminescent spectroscopy be examined to measure local chemical species concentrations as well as temperature profiles in flames of this type. This technique has recently been developed and used successfully on several chemical laser programs at TRW. Its chief advantage lies in being able to make the measurement remotely without disturbing the flow.

REFERENCES

1. F. J. Weyl, "Analytical Methods in Optical Examination of Supersonic Flow," Navord Report 211-45, Navy Department Bureau of Ordnance, Washington, D.C., 11 December 1945.
2. A. B. Witte, "Three Dimensional Flow Field Analysis by a Holographic Interferometry," Final Technical Report, TRW Report No. 12414-6005-R0-00, 15 February 1971.
3. R. D. Matulka and D. J. Collins, "Determination of Three-Dimensional Density Fields from Holographic Interferograms," Journal of Applied Physics, 42, 1109, March 1971.
4. A. B. Witte and B. J. Matthews, "Laser Holography Study of Oil-Fired Burner Combustion," EPA Contract CPA 70-4, TRW Report No. 14103-604-R0-00.
5. A. G. Gaydon and H. G. Wolfhard, Flames, Their Structure, Radiation and Temperature, 3rd edition, Chapman and Hall Ltd., London, pp. 288-304, 1970.
6. R. Friedman and J. B. Levy, Combustion and Flames, 7, 195, 1963.

TECHNICAL REPORT DATA <i>(Please read Instructions on the reverse before completing)</i>		
1. REPORT NO. EPA-650/2-74-031-a	2.	3. RECIPIENT'S ACCESSION NO.
4. TITLE AND SUBTITLE Application of Holographic Methods to the Measurement of Flames and Particulate, Volume I		5. REPORT DATE April 1974
7. AUTHOR(S) A. B. Witte and D. E. Haflinger		6. PERFORMING ORGANIZATION CODE 11982
9. PERFORMING ORGANIZATION NAME AND ADDRESS TRW Systems Group One Space Park Redondo Beach, CA 90278		8. PERFORMING ORGANIZATION REPORT NO. 23523-6001-TU-00
12. SPONSORING AGENCY NAME AND ADDRESS EPA, Office of Research and Development NERC-RTP, Control Systems Laboratory Research Triangle Park, NC 27711		10. PROGRAM ELEMENT NO. LAB014; ROAP 21ADG-51
		11. CONTRACT/GRANT NO. 68-02-0603
		13. TYPE OF REPORT AND PERIOD COVERED Final
		14. SPONSORING AGENCY CODE
15. SUPPLEMENTARY NOTES		
16. ABSTRACT The report gives results of the application of a pulsed ruby laser holographic interferometer to the study of flames, in hopes of extracting temperature profile data. The principle involved is to record holographically the interferogram which presents a three-dimensional record of the interference fringe pattern. The density profile and hence the temperature profile can be calculated from the fringe shift information. The report presents data for a methane-air burner operating both as a diffusion flame and as a premixed flame. The large number of fringe shifts recorded on an interferogram complicated the reduction of the methane-air data, but it was possible to correlate the interferometrically derived temperature data with thermocouple measurements. Application of the technique to a 0.2 gal./hr oil burner was unsuccessful because the highly turbulent flame caused an interference pattern that could not be deciphered.		
17. KEY WORDS AND DOCUMENT ANALYSIS		
a. DESCRIPTORS	b. IDENTIFIERS/OPEN ENDED TERMS	c. COSATI Field/Group
Air Pollution Diffusion Flames Holography Interferometers Temperature Measurement Flame Photometry Combustion	Air Pollution Control Holographic Interferometry Flame Measurement Combustion Research Premixed Flames	13B 14B 20F 21B
18. DISTRIBUTION STATEMENT Unlimited	19. SECURITY CLASS (<i>This Report</i>) Unclassified	21. NO. OF PAGES 69
	20. SECURITY CLASS (<i>This page</i>) Unclassified	22. PRICE